CHAPTER 3

Molecular Properties through Polarizable Embedding

Jógvan Magnus Haugaard Olsen[a] and **Jacob Kongsted**[a]

Contents

Abstract We review the theory related to the calculation of electric and magnetic molecular properties through polarizable embedding. In particular, we derive the expressions for the response functions up to the level of cubic response within the density functional theory-based polarizable embedding (PE-DFT) formalism. In addition, we discuss some illustrative applications related to the calculation of nuclear magnetic resonance parameters, nonlinear optical properties, and electronic excited states in solution.

[a] Department of Physics and Chemistry, University of Southern Denmark, Odense M, Denmark
E-mail address: kongsted@ifk.sdu.dk (Jacob Kongsted)

Advances in Quantum Chemistry, Volume 61
ISSN 0065-3276, DOI: 10.1016/B978-0-12-386013-2.00003-6

1. INTRODUCTION

Accurate modeling of general molecular properties, for example properties related either to molecular ground or excited states, of large molecules or molecular samples currently represents one of the greatest and most significant challenges to modern quantum chemistry. Direct determination of molecular properties, without relying on any parametrized or fitting procedures, requires the use of quantum mechanics. However, from a chemical point of view, it is well recognized that in many cases, the physical changes, for example a chemical reaction or a physical absorption of light, are well localized within some part of the total molecular system. This fact gives rise to the introduction of molecular subsystems in the sense that one subsystem may be more important to describe accurately than another and specifically that the use of quantum mechanics might only be needed in one or a small number of these subsystems. This is, for example, the case when dealing with a solute–solvent system or in more general terms a molecule subjected to a structured environment. In these cases, the part of the system not directly involved in the electronic processes can be described effectively using, for example, classical mechanics. Even though linear scaling techniques are becoming more advanced and may be used to describe larger and more complex systems, effects due to conformational sampling still persist and may become more important as the size of the molecular system is increased. In fact, in many cases, it is mandatory to include effects of nuclear dynamics in combination with the electronic structure in order to pursue a direct comparison with experimental data.

With the aim of addressing large molecular systems, we review a recently developed focused model based on the combined use of quantum mechanics and molecular mechanics (QM/MM) [1–5]. Our approach uses a fully self-consistent polarizable embedding scheme which we denote the PE model [6, 7]. The PE model is generally compatible with any quantum chemical method, but here we focus on its combination with density functional theory (DFT) and time-dependent density functional theory (TD-DFT). The PE method is based on the use of an electrostatic embedding potential which is modeled by localized multipole moment expansions of the molecules, or more generally the fragments, located in the classically treated part of the system. However, the electrostatic embedding potential only accounts for the permanent charge distribution of the environment, and in order to account for many-body induction effects, that is, the polarization of the environment both internally and by the quantum mechanically treated subsystem, we assign a set of localized anisotropic dipole polarizability tensors at the expansion centers giving rise to an induced charge distribution in the environment. The latter is represented in terms of induced dipoles that are determined based on classical response theoretical methods [8]. The localized multipoles and polarizabilities are determined using quantum mechanical methods. The functional form of the polarizable

embedding potential shows some similarities to that of the EFP method by Gordon et al. [9–11]; however, the strength of the PE scheme is the ability to describe excited states and general molecular properties on the same footing as the ground state. This is achieved through a formulation of the PE model within the context of time-dependent quantum mechanical response theory. The PE-DFT model has been implemented up to and including cubic response [6]. This allows for the evaluation of, for example, vertical electronic excitation energies and the related one-, two-, and three-photon transition moments. Furthermore, electronic second-, third-, and fourth-order ground state molecular properties, such as dynamic (second-hyper)polarizabilities, are available, as are excited state first- and second-order molecular properties. In addition, magnetic properties, such as magnetizabilities, nuclear shielding constants, and spin–spin coupling constants, may also be computed, using gauge invariant atomic orbitals (GIAOs) when needed.

Inclusion of nuclear dynamics is of crucial importance especially for larger molecular samples, for example, solutions. Nuclear dynamics is in the present method accounted for by combining the PE scheme with classical molecular dynamics (MD) simulations. This is done in a sequential manner, that is, we first perform MD simulations, and then using an appropriate number of configurations extracted from the MD simulations, we simulate the electronic structure. Thereby, we neglect the effect of the electronic structure on the configurations, and the accuracy of our approach relies first of all on the use of an accurate classical potential to be used for the MD simulations. Inclusion of explicit polarization into force field methods have in recent years received much attention [12]. The current status is that polarization may contribute significantly and specifically to specific solvation processes. For example, polarization causes a significant increase in the dipole moment of a water molecule in the liquid state and may in addition constitute as much as 50% of the total interaction energy [13]. An important point that is followed within the present PE scheme is to be able to calculate all properties characterizing the intermolecular interactions by quantum mechanical methods.

In the following, we will first present a formal derivation of the general PE equations rooted in intermolecular perturbation theory. Next follows a derivation of the PE scheme within the concepts of time-dependent density functional theory, and finally, we present a few illustrative examples. The PE model has been implemented in the Dalton program package [14].

2. THEORETICAL BASIS FOR POLARIZABLE EMBEDDING

The objective of the PE model is to incorporate the effects from a medium into the electronic density of a central molecular core so as to keep the computational cost low while still retaining good accuracy. This is achieved

through the PE potential operator. We begin by considering a simple supermolecular system which we divide into two fragments A and B. The final equations for the supermolecular system are easily generalized to molecular systems with any number of fragments. Fragment A consists of M_{A} nuclei and fragment B consists of M_{B} nuclei. The derivations are carried out using the second quantization formalism [15]. The total nonrelativistic electronic Hamiltonian for the supermolecular system can be written as

$$\hat{H} = \hat{H}^{\mathrm{A}} + \hat{H}^{\mathrm{B}} + \hat{V}^{\mathrm{AB}}, \tag{1}$$

where $\hat{H}^{\mathrm{A}}$ and $\hat{H}^{\mathrm{B}}$ are the fragment Hamiltonians, which contain terms that are specific to fragment A and B, respectively, and $\hat{V}^{\mathrm{AB}}$ is the Coulomb interaction Hamiltonian, which contains all terms related to the interactions between the two fragments. The fragment Hamiltonians are defined as

$$\hat{H}^{i} = \sum_{pq} h^{i}_{pq} \hat{E}^{i}_{pq} + \frac{1}{2} \sum_{pqrs} g^{i}_{pqrs} \hat{e}^{i}_{pqrs} + V^{i}_{\mathrm{nuc}}, \tag{2}$$

where $i = \mathrm{A}$ or B. Here, h_{pq} is an integral over the kinetic energy and nuclear–electron attraction operators, g_{pqrs} is an integral over the electron–electron repulsion operator, and V_{nuc} is the nuclear–nuclear repulsion energy.

Before we define the interaction Hamiltonian, it is convenient first to define the wavefunction of the supermolecular system. We assume that the fragment wavefunctions in isolated form are known, that is,

$$\hat{H}^{\mathrm{A}}|\mathrm{A}\rangle = E^{\mathrm{A}}|\mathrm{A}\rangle \quad \text{and} \quad \hat{H}^{\mathrm{B}}|\mathrm{B}\rangle = E^{\mathrm{B}}|\mathrm{B}\rangle, \tag{3}$$

and that they are individually normalized

$$\langle \mathrm{A}|\mathrm{A}\rangle = 1 \quad \text{and} \quad \langle \mathrm{B}|\mathrm{B}\rangle = 1. \tag{4}$$

The wavefunctions can be expressed as a wave operator acting on the vacuum state

$$|\mathrm{A}\rangle = \hat{\psi}^{\mathrm{A}}|vac\rangle \quad \text{and} \quad |\mathrm{B}\rangle = \hat{\psi}^{\mathrm{B}}|vac\rangle. \tag{5}$$

The form of the wave operators need not be defined, but, in principle, they can describe any type of wavefunction, for example, Hartree–Fock or coupled-cluster wavefunctions. However, at their core, they always consist of strings of creation operators. We define the supermolecular wavefunction as

$$|\mathrm{AB}\rangle = \hat{\psi}^{\mathrm{A}}\hat{\psi}^{\mathrm{B}}|vac\rangle, \tag{6}$$

which is a simple product between the fragment wavefunctions because we require that the following commutation property is fulfilled

$$[\hat{\psi}^{\mathrm{A}}, \hat{\psi}^{\mathrm{B}}] = 0. \tag{7}$$

This corresponds to the assumption that there is no overlap between the wavefunctions of fragments A and B, thereby neglecting exchange and charge-transfer effects between the fragments. This is, in most cases, a reasonable approximation if the distance between the fragments is large but will introduce increasingly larger errors with shorter distances. The underlying commutation rules that apply to the elementary operators are

$$\left[\hat{a}^{\dagger\mathrm{A}}_{p\sigma}, \hat{a}^{\dagger\mathrm{B}}_{q\tau}\right] = \left[\hat{a}^{\mathrm{A}}_{p\sigma}, \hat{a}^{\mathrm{B}}_{q\tau}\right] = \left[\hat{a}^{\dagger\mathrm{A}}_{p\sigma}, \hat{a}^{\mathrm{B}}_{q\tau}\right] = 0, \tag{8}$$

that is, the elementary operators that belong to different fragments commute. Within each fragment, however, the elementary operators obey the usual anticommutation rules.

We are now ready to define the interaction Hamiltonian as

$$\hat{V}^{\mathrm{AB}} = \sum_{pq\in\mathrm{A}} v^{\mathrm{AB}}_{pq}\hat{E}^{\mathrm{A}}_{pq} + \sum_{rs\in\mathrm{B}} v^{\mathrm{AB}}_{rs}\hat{E}^{\mathrm{B}}_{rs} + \sum_{\substack{pq\in\mathrm{A}\\ rs\in\mathrm{B}}} v^{\mathrm{AB}}_{pq,rs}\hat{E}^{\mathrm{A}}_{pq}\hat{E}^{\mathrm{B}}_{rs} + v^{\mathrm{AB}}_{\mathrm{nuc}}, \tag{9}$$

which contains terms that account for nuclear–electron attraction, electron–electron repulsion, and nuclear–nuclear repulsion between the two fragments. Here, we have used the commutation rule defined in Eq. (8) to simplify the two-electron part of the interaction Hamiltonian. The v^{AB}_{pq} factor is an integral over the nuclear–electron attraction operator where the electrons belong to fragment A and the nuclei to fragment B, and it is defined as

$$v^{\mathrm{AB}}_{pq} = -\sum_{m=1}^{M_{\mathrm{B}}} \int \phi^{\mathrm{A}*}_{p}(\mathbf{r}) \frac{Z^{\mathrm{B}}_{m}}{|\mathbf{r}-\mathbf{R}_{m}|} \phi^{\mathrm{A}}_{q}(\mathbf{r}) \mathrm{d}\mathbf{r} = -\sum_{m=1}^{M_{\mathrm{B}}} \int \frac{\rho^{\mathrm{A}}_{pq}(\mathbf{r}) Z^{\mathrm{B}}_{m}}{|\mathbf{r}-\mathbf{R}_{m}|} \mathrm{d}\mathbf{r}. \tag{10}$$

The above equation implicitly defines our use of ρ^{A}_{pq}. Conversely, v^{AB}_{rs} is an integral over the nuclear–electron attraction operator where the electrons belong to fragment B and the nuclei to fragment A, and it is therefore given by

$$v^{\mathrm{AB}}_{rs} = -\sum_{n=1}^{M_{\mathrm{A}}} \int \phi^{\mathrm{B}*}_{r}(\mathbf{r}) \frac{Z^{\mathrm{A}}_{n}}{|\mathbf{R}_{n}-\mathbf{r}|} \phi^{\mathrm{B}}_{s}(\mathbf{r}) \mathrm{d}\mathbf{r} = -\sum_{n=1}^{M_{\mathrm{A}}} \int \frac{Z^{\mathrm{A}}_{n} \rho^{\mathrm{B}}_{rs}(\mathbf{r})}{|\mathbf{R}_{n}-\mathbf{r}|} \mathrm{d}\mathbf{r}, \tag{11}$$

which again implicitly defines our use of ρ^{B}_{rs}. The $v^{\mathrm{AB}}_{pq,rs}$ integral is over the electron–electron repulsion operator where the electrons always belong to

different fragments, and it is defined as

$$v^{\mathrm{AB}}_{pq,rs} = \iint \phi^{\mathrm{A}*}_p(\mathbf{r})\phi^{\mathrm{B}*}_r(\mathbf{r}')\frac{1}{|\mathbf{r}-\mathbf{r}'|}\phi^{\mathrm{A}}_q(\mathbf{r})\phi^{\mathrm{B}}_s(\mathbf{r}')\mathrm{d}\mathbf{r}\mathrm{d}\mathbf{r}'. \tag{12}$$

However, since we are using a product wavefunction of nonoverlapping fragment wavefunctions, this is a purely Coulombic integral. Therefore, we can immediately rewrite it to

$$v^{\mathrm{AB}}_{pq,rs} = \iint \rho^{\mathrm{A}}_{pq}(\mathbf{r})\frac{1}{|\mathbf{r}-\mathbf{r}'|}\rho^{\mathrm{B}}_{rs}(\mathbf{r}')\mathrm{d}\mathbf{r}\mathrm{d}\mathbf{r}', \tag{13}$$

which describes the purely Coulombic interactions between the electronic densities of fragment A and B. Finally, the $v^{\mathrm{AB}}_{\mathrm{nuc}}$ term is the nuclear–nuclear repulsion energy defined as

$$v^{\mathrm{AB}}_{\mathrm{nuc}} = \sum_{n=1}^{M_{\mathrm{A}}}\sum_{m=1}^{M_{\mathrm{B}}}\frac{Z^{\mathrm{A}}_n Z^{\mathrm{B}}_m}{|\mathbf{R}_n - \mathbf{R}_m|}. \tag{14}$$

We now turn our focus on one of the fragments, which we arbitrarily choose as fragment A, and we want to describe the interaction effects from fragment B on this central core. A Rayleigh–Schrödinger perturbation treatment of the supermolecular system, where the interaction Hamiltonian $\hat{V}^{\mathrm{AB}}$ acts as the perturbation, allows us to derive equations for the main contributions to the interaction energy. The energy up to second order in the perturbation is given by

$$E^{(0)} = \langle \mathrm{AB}|\hat{H}^{\mathrm{A}} + \hat{H}^{\mathrm{B}}|\mathrm{AB}\rangle = \langle \mathrm{A}|\hat{H}^{\mathrm{A}}|\mathrm{A}\rangle + \langle \mathrm{B}|\hat{H}^{\mathrm{B}}|\mathrm{B}\rangle \tag{15}$$

$$E^{(1)} = \langle \mathrm{AB}|\hat{V}^{\mathrm{AB}}|\mathrm{AB}\rangle \tag{16}$$

$$E^{(2)} = -\sum_{\substack{ij,\\ i+j\neq 0}} \frac{\langle \mathrm{AB}|\hat{V}^{\mathrm{AB}}|\mathrm{A}^i\mathrm{B}^j\rangle\langle \mathrm{A}^i\mathrm{B}^j|\hat{V}^{\mathrm{AB}}|\mathrm{AB}\rangle}{\epsilon^{\mathrm{AB}}_{ij} - \epsilon^{\mathrm{AB}}_{00}}, \tag{17}$$

which we will use to obtain approximated energy expressions from which we will ultimately derive an effective operator. Thereby, we incorporate effects that lead to the first- and second-order energies into the electron density of the central core. We are only interested in the first- and second-order energies since the zeroth-order energy is simply a sum of the energies of the isolated fragments.

To proceed, we want to eliminate the wavefunction belonging to fragment B. Our strategy is to recast the interaction Hamiltonian using a Taylor

series expansion of $|\mathbf{r}-\mathbf{r}'|^{-1}$ and $|\mathbf{r}-\mathbf{R}_m|^{-1}$ around an origin $\mathbf{R}_o$ located inside fragment B. Here, $\mathbf{r}'$ and $\mathbf{R}_m$ are electronic and nuclear coordinates, respectively, belonging to fragment B; the point $\mathbf{r}$ is, for now, an arbitrary point outside the charge distribution of fragment B. Later, $\mathbf{r}$ will either refer to an electronic or nuclear coordinate inside the central core system. The expansion of $|\mathbf{r}-\mathbf{r}'|^{-1}$ can be written in closed form using a multi-index notation

$$\frac{1}{|\mathbf{r}-\mathbf{r}'|}=\sum_{|k|=0}^{\infty}\frac{(-1)^{|k|}}{k!}\left(\nabla^k\frac{1}{|\mathbf{r}-\mathbf{R}_o|}\right)\left(\mathbf{r}'-\mathbf{R}_o\right)^k \tag{18}$$

where the multi-index $k=(k_x,k_y,k_z)$ is a 3-tuple of nonnegative integers, $|k|=k_x+k_y+k_z$ and ∇^k is defined as the multi-index power of the partial derivative operator

$$\nabla^k=\left(\frac{\partial}{\partial r_x}\right)^{k_x}\left(\frac{\partial}{\partial r_y}\right)^{k_y}\left(\frac{\partial}{\partial r_z}\right)^{k_z}. \tag{19}$$

For each value of $|k|$, the summation in Eq. (18) is over $3^{|k|}$ elements; for example, for $|k|=1$, the summation is over three elements, namely, $(1,0,0)$, $(0,1,0)$, and $(0,0,1)$, which represent the x, y, and z components, respectively. The multi-index also specifies the Cartesian component, for example, $k=(2,1,0)$ is the xxy component. The convergence of the expansion depends on the distance from the origin to $\mathbf{r}$ relative to the extent of the charge distribution of both fragments. At large distances, it usually converges rapidly but worsens as the distance becomes shorter and can even diverge at short distances. Using distributed multipole expansions of the charge distribution improves the convergence; however, at very short distances, the error from the expansion will still be significant.

In Eq. (18), we recognize the first quantization kth-order electronic multipole moment operator $(\mathbf{r}'-\mathbf{R}_o)^k$. An analogous expansion of $|\mathbf{r}-\mathbf{R}_m|^{-1}$ would yield the nuclear multipole moment operator $(\mathbf{R}_m-\mathbf{R}_o)^k$. The higher-order multipole moments generally depend on the choice of origin; however, to simplify the notation, we omit any explicit reference to this dependence. The partial derivatives in Eq. (18) are elements of the so-called interaction tensors defined as

$$T^{(k)}_{AB}(\mathbf{r})=\nabla^k\frac{1}{|\mathbf{r}-\mathbf{R}_o|}. \tag{20}$$

The multi-index in parentheses, used as superscript on the tensor, is actually the norm $|k|$; however, since it also specifies the rank of the tensor, and therefore we use a special notation.

We can now rewrite the interaction Hamiltonian by replacing all occurrences of $|\mathbf{r}-\mathbf{r}'|^{-1}$ and $|\mathbf{r}-\mathbf{R}_m|^{-1}$ in Eqs. (10, 11, 13, and 14) with the

appropriate Taylor expansion. The interaction Hamiltonian is thereby redefined to

$$\hat{V}^{\mathrm{AB}} = \sum_{|k|=0}^{\infty} \frac{(-1)^{|k|}}{k!} \hat{F}_{\mathrm{A}}^{(k)} \hat{Q}_{\mathrm{B}}^{(k)}, \tag{21}$$

where $\hat{F}_{\mathrm{A}}^{(k)}$ and $\hat{Q}_{\mathrm{B}}^{(k)}$ act on the wavefunctions belonging to fragment A and B, respectively. The $\hat{F}_{\mathrm{A}}^{(k)}$ operator is defined as

$$\hat{F}_{\mathrm{A}}^{(k)} = F_{\mathrm{A,nuc}}^{(k)} + \hat{F}_{\mathrm{A,el}}^{(k)} = \sum_{n=1}^{M_{\mathrm{A}}} Z_n^{\mathrm{A}} T_{\mathrm{AB}}^{(k)}(\mathbf{R}_n) - \sum_{pq \in \mathrm{A}} \left(\int \rho_{pq}^{\mathrm{A}}(\mathbf{r}) T_{\mathrm{AB}}^{(k)}(\mathbf{r}) \mathrm{d}\mathbf{r} \right) \hat{E}_{pq}^{\mathrm{A}}, \tag{22}$$

the expectation value of which gives the electrostatic potential, electric field, and field gradient for $|k| = 0, 1, 2$, respectively. The $\hat{Q}_{\mathrm{B}}^{(k)}$ operator is the multipole moment operator defined as

$$\begin{aligned} \hat{Q}_{\mathrm{B}}^{(k)} = Q_{\mathrm{B,nuc}}^{(k)} + \hat{Q}_{\mathrm{B,el}}^{(k)} = & \sum_{m=1}^{M_{\mathrm{B}}} Z_m^{\mathrm{B}} \left(\mathbf{R}_{\mathrm{m}} - \mathbf{R}_{\mathrm{o}}\right)^k \\ & - \sum_{rs \in \mathrm{B}} \left(\int \rho_{rs}^{\mathrm{B}}(\mathbf{r}') \left(\mathbf{r}' - \mathbf{R}_{\mathrm{o}}\right)^k \mathrm{d}\mathbf{r}' \right) \hat{E}_{rs}^{\mathrm{B}}. \end{aligned} \tag{23}$$

Using the redefined interaction Hamiltonian, the first-order energy (Eq. (16)) yields

$$E_{\mathrm{es}}^{\mathrm{AB}} = \langle \mathrm{AB} | \hat{V}^{\mathrm{AB}} | \mathrm{AB} \rangle = \sum_{|k|=0}^{\infty} \frac{(-1)^{|k|}}{k!} \left(F_{\mathrm{A,nuc}}^{(k)} + \langle \mathrm{A} | \hat{F}_{\mathrm{A,el}}^{(k)} | \mathrm{A} \rangle \right) Q_{\mathrm{B}}^{(k)}, \tag{24}$$

which is the electrostatic interaction energy given in terms of the multipole moments $Q_{\mathrm{B}}^{(k)}$ of fragment B. The definition of the electrostatic energy given in Eq. (24) will be used to construct an effective operator so that this effect is incorporated directly in the electron density of the central core fragment.

The second-order energy (Eq. (17)) needs further breakdown before we can identify the relevant energy contributions we need. First of all, we see that it is expressed as a sum-over-states that includes all terms except when both fragments A and B are in their ground state, that is, $i = 0$ and $j = 0$. It is therefore possible to separate it into three different contributions: two of which only include excited states in one fragment, these are the induction energy terms, and one which includes excited states in both fragments simultaneously, which is the dispersion energy [16]. Although the

dispersion energy can be important, it is neglected in our model since there is no straightforward way of including it in operator form. The induction energy of fragment A can be rewritten in terms of the multipole moments of fragment B using the interaction Hamiltonian as defined in Eqs. (21–23)

$$E_{\mathrm{ind}}^{\mathrm{A}} = -\sum_{i\neq 0} \frac{\langle \mathrm{AB}|\hat{V}^{\mathrm{AB}}|\mathrm{A}^i\mathrm{B}\rangle\langle \mathrm{A}^i\mathrm{B}|\hat{V}^{\mathrm{AB}}|\mathrm{AB}\rangle}{\epsilon_i^{\mathrm{A}} - \epsilon_0^{\mathrm{A}}}. \tag{25}$$

Taking the expectation value with respect to the wavefunction belonging to fragment B yields

$$E_{\mathrm{ind}}^{\mathrm{A}} = -\sum_{|k|=0}^{\infty} \frac{(-1)^{|k|}}{k!} Q_{\mathrm{B}}^{(k)} \sum_{i\neq 0} \frac{\langle \mathrm{A}|\hat{F}_{\mathrm{A}}^{(k)}|\mathrm{A}^i\rangle\langle \mathrm{A}^i|\hat{F}_{\mathrm{A}}^{(k)}|\mathrm{A}\rangle}{\epsilon_i^{\mathrm{A}} - \epsilon_0^{\mathrm{A}}} Q_{\mathrm{B}}^{(k)}, \tag{26}$$

which is the interaction energy due to the polarization of fragment A by the multipole moments of fragment B in its ground state. In our model, this energy contribution is implicitly included via the use of an effective operator that includes the multipole moments of fragment B, thus polarizing the electron density of fragment A. The induction energy of fragment B is defined analogous to the induction energy of fragment A

$$E_{\mathrm{ind}}^{\mathrm{B}} = -\sum_{j\neq 0} \frac{\langle \mathrm{AB}|\hat{V}^{\mathrm{AB}}|\mathrm{AB}^j\rangle\langle \mathrm{AB}^j|\hat{V}^{\mathrm{AB}}|\mathrm{AB}\rangle}{\epsilon_j^{\mathrm{B}} - \epsilon_0^{\mathrm{B}}}, \tag{27}$$

which we can rewrite to

$$E_{\mathrm{ind}}^{\mathrm{B}} = -\sum_{|k|=0}^{\infty} \frac{(-1)^{|k|}}{k!} \langle \mathrm{A}|\hat{F}_{\mathrm{A}}^{(k)}|\mathrm{A}\rangle \sum_{j\neq 0} \frac{\langle \mathrm{B}|\hat{Q}_{\mathrm{B}}^{(k)}|\mathrm{B}^j\rangle\langle \mathrm{B}^j|\hat{Q}_{\mathrm{B}}^{(k)}|\mathrm{B}\rangle}{\epsilon_j^{\mathrm{B}} - \epsilon_0^{\mathrm{B}}} \langle \mathrm{A}|\hat{F}_{\mathrm{A}}^{(k)}|\mathrm{A}\rangle. \tag{28}$$

We recognize the sum-over-states part of the expression as the polarizabilities of fragment B. Note that the zeroth-order term, where $\hat{Q}_{\mathrm{B}}^{(0)} = q_{\mathrm{B}}$, does not contribute due to orthogonality. Truncating the expansion at $|k| = 1$, that is, at the dipole level, and evaluating the expectation values yields

$$E_{\mathrm{ind}}^{\mathrm{B}} = -\frac{1}{2}\left(\mathbf{F}_{\mathrm{nuc}}^{\mathrm{A}} + \mathbf{F}_{\mathrm{el}}^{\mathrm{A}}\right)\boldsymbol{\alpha}^{\mathrm{B}}\left(\mathbf{F}_{\mathrm{nuc}}^{\mathrm{A}} + \mathbf{F}_{\mathrm{el}}^{\mathrm{A}}\right) = -\frac{1}{2}\left(\mathbf{F}_{\mathrm{nuc}}^{\mathrm{A}} + \mathbf{F}_{\mathrm{el}}^{\mathrm{A}}\right)\boldsymbol{\mu}_{\mathrm{ind}}^{\mathrm{B}}(\mathbf{F}_{\mathrm{tot}}), \tag{29}$$

where $\left(\mathbf{F}_{\mathrm{nuc}}^{\mathrm{A}} + \mathbf{F}_{\mathrm{el}}^{\mathrm{A}}\right)$ is the electric field due to the nuclei and electrons, respectively, in fragment A and $\boldsymbol{\mu}_{\mathrm{ind}}^{\mathrm{B}}(\mathbf{F}_{\mathrm{tot}})$ is the dipole moment induced by the total electric field $\mathbf{F}_{\mathrm{tot}}$. In this case, the total electric field stems only from the

nuclei and electrons in fragment A. Generally, however, it is a sum of all electric fields including the field from other induced dipoles. This is a classical energy expression which we use to allow polarization of fragment B by the electrons and nuclei in fragment A. The induction energy is nonadditive due to the mutual polarization and therefore has to be solved for self-consistently.

We now have the energy expression needed to derive a generalized PE potential operator within a given QM formalism. For a system consisting of any number of fragments, where one is chosen as the central core system and the other fragments are represented by a multicenter multipole moment expansion and distributed dipole–dipole polarizability tensors, the relevant energy is given by

$$E_{\text{tot}}^{\text{PE}} = E_{\text{QM}}^{\text{PE}} + E_{\text{es}}^{\text{PE}} + E_{\text{ind}}^{\text{PE}}. \tag{30}$$

The $E_{\text{QM}}^{\text{PE}}$ term is the energy of the isolated core fragment evaluated at a given level of theory, and $E_{\text{es}}^{\text{PE}}$ is the electrostatic interaction energy given by

$$E_{\text{es}}^{\text{PE}} = \sum_{s=1}^{S} \sum_{|k|=0}^{K} \frac{(-1)^{|k|}}{k!} \left(F_{s,\text{nuc}}^{(k)} + \langle 0|\hat{F}_{s,\text{el}}^{(k)}|0\rangle \right) Q_s^{(k)}, \tag{31}$$

where we have introduced the truncation level K and summation over S sites in the surrounding fragments. The nuclear contribution $F_{s,\text{nuc}}^{(k)}$ is defined as

$$F_{s,\text{nuc}}^{(k)} = \sum_{n=1}^{M} Z_n T_{ns}^{(k)}(\mathbf{R}_n), \tag{32}$$

and the electronic contribution is given by the expectation value over the operator $\hat{F}_{s,\text{el}}^{(k)}$, which is defined by

$$\hat{F}_{s,\text{el}}^{(k)} = \sum_{pq} t_{s,pq}^{(k)} \hat{E}_{pq}, \tag{33}$$

where the $t_{s,pq}^{(k)}$ integral is defined as

$$t_{s,pq}^{(k)} = -\int \rho_{pq}(\mathbf{r}) T_s^{(k)}(\mathbf{r}) \mathrm{d}\mathbf{r}. \tag{34}$$

The subindices on the interaction tensors specify which position vectors it contains, for example, $T_{ns}^{(k)} = \nabla^k \frac{1}{|\mathbf{R}_n - \mathbf{R}_s|}$. One index implicitly specifies that the other coordinate is an electron coordinate, for example, $T_s^{(k)} = \nabla^k \frac{1}{|\mathbf{r} - \mathbf{R}_s|}$. The

induction energy $E_{\text{ind}}^{\text{PE}}$ due to the polarization of the surrounding fragments is given by

$$E_{\text{ind}}^{\text{PE}} = -\frac{1}{2}\sum_{s=1}^{S}\left(\mathbf{F}_{\text{nuc}} + \mathbf{F}_{\text{el}} + \mathbf{F}_{\text{mul}}\right)\boldsymbol{\mu}_s^{\text{ind}}(\mathbf{F}_{\text{tot}}), \tag{35}$$

where the additional electric field, $\mathbf{F}_{\text{mul}}$, stems from the multipole moments of all the other fragments and the total electric field $\mathbf{F}_{\text{tot}}$ is a sum of contributions from the electrons and nuclei in the central core and the multipole moments and induced dipoles from all other fragments. An induced dipole moment is given by

$$\boldsymbol{\mu}_s^{\text{ind}}(\mathbf{F}_{\text{tot}}) = \boldsymbol{\alpha}_s\mathbf{F}_{\text{tot}} = \boldsymbol{\alpha}_s\left(\mathbf{F}_{\text{nuc}} + \mathbf{F}_{\text{el}} + \mathbf{F}_{\text{mul}} + \mathbf{F}_{\text{ind}}\right), \tag{36}$$

where the electric field from the other induced dipoles $\mathbf{F}_{\text{ind}}$ is given by

$$\mathbf{F}_{\text{ind}} = \sum_{s'\neq s}^{S}\mathbf{T}_{s'}^{(2)}\boldsymbol{\mu}_{s'}^{\text{ind}}(\mathbf{F}_{\text{tot}}). \tag{37}$$

Inserting Eq. (37) into Eq. (36) and summing over all sites yields a system of coupled equations

$$\sum_{s}^{S}\boldsymbol{\mu}_s^{\text{ind}}(\mathbf{F}_{\text{tot}}) = \sum_{s}^{S}\boldsymbol{\alpha}_s\left(\mathbf{F}_{\text{nem}} + \sum_{s'\neq s}^{S}\mathbf{T}_{s'}^{(2)}\boldsymbol{\mu}_{s'}^{\text{ind}}(\mathbf{F}_{\text{tot}})\right), \tag{38}$$

where the electric field from all sources, except induced dipoles, has been collected in a single term $\mathbf{F}_{\text{nem}} = \mathbf{F}_{\text{nuc}} + \mathbf{F}_{\text{el}} + \mathbf{F}_{\text{mul}}$. The induced dipole moments can be solved for iteratively using the Jacobi method or directly through matrix-vector multiplication using the equation given by

$$\boldsymbol{\mu}^{\text{ind}} = \mathbf{B}\mathbf{F}, \tag{39}$$

where $\mathbf{B}$ is the symmetric $3S \times 3S$-dimensional classical response matrix [8] connecting the electric fields and the set of induced dipoles

$$\boldsymbol{\mu}^{\text{ind}} = \begin{pmatrix} \boldsymbol{\mu}_1^{\text{ind}} \\ \boldsymbol{\mu}_2^{\text{ind}} \\ \vdots \\ \boldsymbol{\mu}_S^{\text{ind}} \end{pmatrix}. \tag{40}$$

The response matrix is defined as

$$\mathbf{B} = \begin{pmatrix} \boldsymbol{\alpha}_1^{-1} & \mathbf{T}_{12}^{(2)} & \cdots & \mathbf{T}_{1S}^{(2)} \\ \mathbf{T}_{21}^{(2)} & \boldsymbol{\alpha}_2^{-1} & \ddots & \vdots \\ \vdots & \ddots & \ddots & \mathbf{T}_{(S-1)S}^{(2)} \\ \mathbf{T}_{S1}^{(2)} & \cdots & \mathbf{T}_{S(S-1)}^{(2)} & \boldsymbol{\alpha}_S^{-1} \end{pmatrix}^{-1}, \tag{41}$$

where the diagonal blocks contain the inverse polarizability tensors and the off-diagonal blocks are rank 2 interaction tensors.

2.1. Polarizable embedding applied to density functional theory

The PE-DFT method is derived by constructing an effective Kohn–Sham (KS) operator, that is,

$$\hat{f}_{\text{eff}} = \hat{f}_{\text{KS}} + \hat{v}_{\text{PE}}, \tag{42}$$

where $\hat{f}_{\text{KS}}$ is the ordinary vacuum KS operator and $\hat{v}_{\text{PE}}$ is the PE potential operator. The contributions to the effective KS operator is determined by minimization of the energy with respect to the electron density. Therefore, we only need to consider terms that depend on the electron density, that is, the electronic parts of the electrostatic interaction energy (Eq. (31)) and the induction energy (Eq. (35)), keeping in mind that the induced dipoles also depend on the density through the electric field. Thus, the PE potential operator is found to be

$$\hat{v}_{\text{PE}} = \sum_{s=1}^{S} \sum_{|k|=0}^{K} \frac{(-1)^{|k|}}{k!} Q_s^{(k)} \hat{F}_{s,\text{el}}^{(k)} - \sum_{s=1}^{S} \boldsymbol{\mu}_s^{\text{ind}}(\mathbf{F}_{\text{tot}}) \hat{\mathbf{F}}_{s,\text{el}}^{(1)}, \tag{43}$$

where the induced dipole moments need to be updated in each self-consistent field (SCF) iteration due to the density dependence, thus leading to a fully self-consistent treatment of the polarization.

2.2. Polarizable embedding within response theory

Here, we provide the theoretical basis for incorporating the PE potential in quantum mechanical response theory, including the derivation of the contributions to the linear, quadratic, and cubic response functions. The derivations follow closely the formulation of linear and quadratic response theory within DFT by Sałek et al. [17] and cubic response within DFT by Jansik et al. [18] Furthermore, the derived equations show some similarities to other response-based environmental methods, for example, the polarizable continuum model [19, 20] (PCM) or the spherical cavity dielectric

continuum approach [21, 22]. This is not surprising since these two methods also explicitly include the polarizable nature of the surrounding. Physically, both the PE and dielectric continuum models are furthermore based on the use of a nonlinear effective Hamiltonian.

We start the derivations by considering the expectation value of a time-independent operator $\hat{A}$ which is expanded in orders of a time-dependent perturbation

$$\langle t|\hat{A}|t\rangle = \langle t|\hat{A}|t\rangle^{(0)} + \langle t|\hat{A}|t\rangle^{(1)} + \langle t|\hat{A}|t\rangle^{(2)} + \langle t|\hat{A}|t\rangle^{(3)} + \cdots . \tag{44}$$

The first term on the right-hand side is the time-independent expectation value, whereas the second, third, and fourth terms describe the linear, quadratic, and cubic response to the perturbation, respectively. The Fourier transformed representations are given by

$$\langle t|\hat{A}|t\rangle^{(1)} = \int \langle\langle \hat{A}; \hat{V}^{\omega_1} \rangle\rangle_{\omega_1} \exp(-i\omega_1 t) \mathrm{d}\omega_1 \tag{45}$$

$$\langle t|\hat{A}|t\rangle^{(2)} = \frac{1}{2} \iint \langle\langle \hat{A}; \hat{V}^{\omega_1}, \hat{V}^{\omega_2} \rangle\rangle_{\omega_1,\omega_2} \exp(-i(\omega_1+\omega_2)t) \mathrm{d}\omega_1 \mathrm{d}\omega_2 \tag{46}$$

$$\begin{aligned}\langle t|\hat{A}|t\rangle^{(3)} = \frac{1}{6} \iiint & \langle\langle \hat{A}; \hat{V}^{\omega_1}, \hat{V}^{\omega_2}, \hat{V}^{\omega_3} \rangle\rangle_{\omega_1,\omega_2,\omega_3} \\ & \times \exp(-i(\omega_1+\omega_2+\omega_3)t) \mathrm{d}\omega_1 \mathrm{d}\omega_2 \mathrm{d}\omega_3,\end{aligned} \tag{47}$$

where $\langle\langle \hat{A}; \hat{V}^{\omega_1} \rangle\rangle_{\omega_1}$, $\langle\langle \hat{A}; \hat{V}^{\omega_1}, \hat{V}^{\omega_2} \rangle\rangle_{\omega_1,\omega_2}$, and $\langle\langle \hat{A}; \hat{V}^{\omega_1}, \hat{V}^{\omega_2}, \hat{V}^{\omega_3} \rangle\rangle_{\omega_1,\omega_2,\omega_3}$ are the linear, quadratic, and cubic response functions, respectively, and the perturbation operator is defined as

$$\hat{V}(t) = \int \hat{V}^{\omega} \exp(-i\omega t) \mathrm{d}\omega. \tag{48}$$

The time development of the molecular orbitals is determined by the time-dependent KS equations

$$\left(\hat{H}(t) + \hat{V}(t)\right)|t\rangle = i\frac{\partial}{\partial t}|t\rangle \tag{49}$$

where $\hat{H}(t)$ is the time-dependent KS Hamiltonian given by

$$\hat{H}(t) = \sum_{pq} f_{pq}(t)\hat{E}_{pq} \tag{50}$$

and $|t\rangle$ is the time-dependent KS determinant. We use an exponential parametrization of the KS determinant

$$|t\rangle = \exp(-\hat{\kappa}(t))|0\rangle \tag{51}$$

where $|0\rangle$ is the unperturbed KS determinant and $\hat{\kappa}(t)$ is the anti-Hermitian time-evolution operator defined as

$$\hat{\kappa}(t) = \sum_{pq} \kappa_{pq}(t)\hat{E}_{pq}, \tag{52}$$

with $\kappa_{pq}(t)$ as the time-dependent variational parameters. Thus, the expectation value over a time-independent operator $\hat{A}$ becomes

$$\langle \hat{A} \rangle = \langle t|\hat{A}|t\rangle = \langle 0| \exp\big(\hat{\kappa}(t)\big)\hat{A} \exp(-\hat{\kappa}(t))|0\rangle \tag{53}$$

which can be expanded using a Baker–Campbell–Hausdorff (BCH) expansion [15]

$$\begin{aligned}\langle \hat{A} \rangle = \langle 0|\hat{A}|0\rangle + \langle 0|[\hat{\kappa}(t), \hat{A}]|0\rangle + \frac{1}{2}\langle 0|[\hat{\kappa}(t), [\hat{\kappa}(t), \hat{A}]]|0\rangle \\ + \frac{1}{6}\langle 0|[\hat{\kappa}(t), [\hat{\kappa}(t), [\hat{\kappa}(t), \hat{A}]]]|0\rangle + \cdots .\end{aligned} \tag{54}$$

The time-evolution operator can be expanded in orders of the perturbation

$$\hat{\kappa}(t) = \hat{\kappa}^{(1)}(t) + \hat{\kappa}^{(2)}(t) + \hat{\kappa}^{(3)}(t) + \cdots \tag{55}$$

with the following representations in frequency space

$$\hat{\kappa}^{(1)}(t) = \int \hat{\kappa}^{\omega_1} \exp(-i\omega_1 t)\mathrm{d}\omega_1 \tag{56}$$

$$\hat{\kappa}^{(2)}(t) = \frac{1}{2}\iint \hat{\kappa}^{\omega_1,\omega_2} \exp(-i(\omega_1 + \omega_2)t)\mathrm{d}\omega_1\mathrm{d}\omega_2 \tag{57}$$

$$\hat{\kappa}^{(3)}(t) = \frac{1}{6}\iiint \hat{\kappa}^{\omega_1,\omega_2,\omega_3} \exp(-i(\omega_1 + \omega_2 + \omega_3)t)\mathrm{d}\omega_1\mathrm{d}\omega_2\mathrm{d}\omega_3. \tag{58}$$

Inserting the expansion of the time-evolution operator (Eq. (55)) into the BCH expansion of the expectation value given in Eq. (54) leads to

$$\begin{aligned}\langle \hat{A} \rangle = \langle 0|\hat{A}|0\rangle + \langle 0|[\hat{\kappa}^{(1)}(t), \hat{A}]|0\rangle + \langle 0|[\hat{\kappa}^{(2)}(t), \hat{A}]|0\rangle + \langle 0|[\hat{\kappa}^{(3)}(t), \hat{A}]|0\rangle \\ + \frac{1}{2}\langle 0|[\hat{\kappa}^{(1)}(t), [\hat{\kappa}^{(1)}(t), \hat{A}]]|0\rangle + \frac{1}{2}\langle 0|[\hat{\kappa}^{(1)}(t), [\hat{\kappa}^{(2)}(t), \hat{A}]]|0\rangle \\ + \frac{1}{2}\langle 0|[\hat{\kappa}^{(2)}(t), [\hat{\kappa}^{(1)}(t), \hat{A}]]|0\rangle + \frac{1}{6}\langle 0|[\hat{\kappa}^{(1)}(t), [\hat{\kappa}^{(1)}(t), [\hat{\kappa}^{(1)}(t), \hat{A}]]]|0\rangle.\end{aligned} \tag{59}$$

From this expression, we can identify terms according to their order in the perturbation as follows:

$$\langle t|\hat{A}|t\rangle^{(1)} = \langle 0|[\hat{\kappa}^{(1)}(t), \hat{A}]|0\rangle \tag{60}$$

$$\langle t|\hat{A}|t\rangle^{(2)} = \langle 0|[\hat{\kappa}^{(2)}(t), \hat{A}]|0\rangle + \frac{1}{2}\langle 0|[\hat{\kappa}^{(1)}(t), [\hat{\kappa}^{(1)}(t), \hat{A}]]|0\rangle \tag{61}$$

$$\begin{aligned}\langle t|\hat{A}|t\rangle^{(3)} = {} & \langle 0|[\hat{\kappa}^{(3)}(t), \hat{A}]|0\rangle + \frac{1}{2}\langle 0|[\hat{\kappa}^{(1)}(t), [\hat{\kappa}^{(2)}(t), \hat{A}]]|0\rangle \\ & + \frac{1}{2}\langle 0|[\hat{\kappa}^{(2)}(t), [\hat{\kappa}^{(1)}(t), \hat{A}]]|0\rangle \\ & + \frac{1}{6}\langle 0|[\hat{\kappa}^{(1)}(t), [\hat{\kappa}^{(1)}(t), [\hat{\kappa}^{(1)}(t), \hat{A}]]]|0\rangle\end{aligned} \tag{62}$$

Comparing Eqs. (60–62) to Eqs. (45–47) shows that the response functions can be obtained by Fourier transformation to the frequency domain. This leads to the following expressions for the response functions up to cubic response

$$\langle\langle \hat{A}; \hat{V}^{\omega_1}\rangle\rangle_{\omega_1} = \langle 0|[\hat{\kappa}^{\omega_1}, \hat{A}]|0\rangle \tag{63}$$

$$\langle\langle \hat{A}; \hat{V}^{\omega_1}, \hat{V}^{\omega_2}\rangle\rangle_{\omega_1,\omega_2} = \langle 0|[\hat{\kappa}^{\omega_1,\omega_2}, \hat{A}]|0\rangle + \hat{P}_{12}\langle 0|[\hat{\kappa}^{\omega_1}, [\hat{\kappa}^{\omega_2}, \hat{A}]]|0\rangle \tag{64}$$

$$\begin{aligned}\langle\langle \hat{A}; \hat{V}^{\omega_1}, \hat{V}^{\omega_2}, \hat{V}^{\omega_3}\rangle\rangle_{\omega_1,\omega_2,\omega_3} = {} & \langle 0|[\hat{\kappa}^{\omega_1,\omega_2,\omega_3}, \hat{A}]|0\rangle \\ & + \frac{3}{2}\hat{P}_{123}\langle 0|[\hat{\kappa}^{\omega_1}, [\hat{\kappa}^{\omega_2,\omega_3}, \hat{A}]]|0\rangle \\ & + \frac{3}{2}\hat{P}_{123}\langle 0|[\hat{\kappa}^{\omega_1,\omega_2}, [\hat{\kappa}^{\omega_3}, \hat{A}]]|0\rangle \\ & + \hat{P}_{123}\langle 0|[\hat{\kappa}^{\omega_1}, [\hat{\kappa}^{\omega_2}, [\hat{\kappa}^{\omega_3}, \hat{A}]]]|0\rangle,\end{aligned} \tag{65}$$

where the symmetrizers $\hat{P}_{12}$ and $\hat{P}_{123}$ have been introduced. The symmetrizers are defined through

$$\hat{P}_{12}A(\omega_1, \omega_2) = \frac{1}{2}\big(A(\omega_1, \omega_2) + A(\omega_2, \omega_1)\big) \tag{66}$$

$$\begin{aligned}\hat{P}_{123}A(\omega_1, \omega_2, \omega_3) = \frac{1}{6}\Big(& A(\omega_1, \omega_2, \omega_3) + A(\omega_1, \omega_3, \omega_2) + A(\omega_2, \omega_1, \omega_3) \\ & + A(\omega_2, \omega_3, \omega_1) + A(\omega_3, \omega_1, \omega_2) + A(\omega_3, \omega_2, \omega_1)\Big),\end{aligned} \tag{67}$$

and they ensure that the response functions satisfy the proper symmetry condition.

The electron density can also be expanded in orders of the perturbation as

$$\rho(\mathbf{r},t) = \sum_n \rho^{(n)}(\mathbf{r},t) = \sum_n \sum_{pq} \phi_p^*(\mathbf{r})\phi_q(\mathbf{r}) D_{pq}^{(n)}, \tag{68}$$

where we can immediately write down the corrections to the density matrix up to third order by using the preceding derivations

$$D_{pq}^{\omega_1} = \langle 0|[\hat{\kappa}^{\omega_1}, \hat{E}_{pq}]|0\rangle \tag{69}$$

$$D_{pq}^{\omega_1,\omega_2} = \langle 0|[\hat{\kappa}^{\omega_1,\omega_2}, \hat{E}_{pq}]|0\rangle + \hat{P}_{12}\langle 0|[\hat{\kappa}^{\omega_1}, [\hat{\kappa}^{\omega_2}, \hat{E}_{pq}]]|0\rangle \tag{70}$$

$$\begin{aligned} D_{pq}^{\omega_1,\omega_2,\omega_3} = {} & \langle 0|[\hat{\kappa}^{\omega_1,\omega_2,\omega_3}, \hat{E}_{pq}]|0\rangle \\ & + \frac{3}{2}\hat{P}_{123}\langle 0|[\hat{\kappa}^{\omega_1}, [\hat{\kappa}^{\omega_2,\omega_3}, \hat{E}_{pq}]]|0\rangle \\ & + \frac{3}{2}\hat{P}_{123}\langle 0|[\hat{\kappa}^{\omega_1,\omega_2}, [\hat{\kappa}^{\omega_3}, \hat{E}_{pq}]]|0\rangle \\ & + \hat{P}_{123}\langle 0|[\hat{\kappa}^{\omega_1}, [\hat{\kappa}^{\omega_2}, [\hat{\kappa}^{\omega_3}, \hat{E}_{pq}]]]|0\rangle. \end{aligned} \tag{71}$$

Finally, we also expand the time-dependent Kohn–Sham Hamiltonian as:

$$\hat{H}(t) = \sum_n \sum_{pq} f_{pq}^{(n)} \hat{E}_{pq} = \sum_n \sum_{pq} \left(\delta_{0n} h_{pq} + j_{pq}^{(n)} + v_{\mathrm{xc},pq}^{(n)} + v_{\mathrm{PE},pq}^{(n)}\right) \hat{E}_{pq}, \tag{72}$$

where h_{pq} is an integral over the kinetic energy and nuclear-attraction operators, $j_{pq}^{(n)}$ is a nth-order Coulomb integral, and $v_{\mathrm{xc},pq}^{(n)}$ is a nth-order integral over the exchange-correlation potential. The final term $v_{\mathrm{PE},pq}^{(n)}$ is a nth-order integral over the PE potential defined as

$$v_{\mathrm{PE},pq}^{(n)} = \delta_{0n} \sum_{s=1}^{S} \sum_{|k|=0}^{K} \frac{(-1)^{|k|}}{k!} Q_s^{(k)} t_{s,pq}^{(k)} - \sum_{s=1}^{S} \boldsymbol{\mu}_s^{\mathrm{ind}}(\mathbf{F}_{\mathrm{tot}}^{(n)}) \mathbf{t}_{s,pq}^{(1)}. \tag{73}$$

For $n > 0$, it is only the induction part of $v_{\mathrm{PE},pq}^{(n)}$ that contributes due to the density dependence in the induced dipoles via the electric fields.

The $\kappa_{pq}(t)$ parameters are obtained through the Ehrenfest theorem which can be written as [23]

$$\langle 0|\left[\hat{\mathbf{q}}, \exp\left(\hat{\kappa}(t)\right)\left(\hat{H}(t) + \hat{V}(t) - i\frac{\mathrm{d}}{\mathrm{d}t}\right)\exp\left(-\hat{\kappa}(t)\right)\right]|0\rangle = 0, \tag{74}$$

where $\hat{\mathbf{q}}$ is a vector collecting all the excitation operators $\hat{E}_{pq}$. Equation (74) is then expanded in a BCH expansion, and the perturbation expansions of the time-evolution operator $\hat{\kappa}(t)$ and the KS Hamiltonian $\hat{H}(t)$ are inserted. Subsequently, terms that are first-, second-, and third-order in the perturbation, respectively, are collected. Thereby, we obtain sets of equations that can be used to determine the variational parameters, thus allowing us to calculate the linear, quadratic, and cubic response functions.

2.2.1. Linear response

Collecting all first-order terms obtained through the BCH expansion of the Ehrenfest theorem given in Eq. (74) leads to a system of differential equations

$$\langle 0|[\hat{\mathbf{q}}, \hat{H}^{(1)} + \hat{V}(t)]|0\rangle + \langle 0|[\hat{\mathbf{q}}, [\hat{\kappa}^{(1)}, \hat{H}^{(0)}]]|0\rangle + i\langle 0|[\hat{\mathbf{q}}, \dot{\hat{\kappa}}^{(1)}]|0\rangle = 0. \tag{75}$$

A Fourier transformation yields a more convenient algebraic equation

$$\langle 0|[\hat{\mathbf{q}}, [\hat{H}^{0}, \hat{\kappa}^{\omega_1}] - \hat{H}^{\omega_1}]|0\rangle - \omega_1 \langle 0|[\hat{\mathbf{q}}, \hat{\kappa}^{\omega_1}]|0\rangle = \langle 0|[\hat{\mathbf{q}}, \hat{V}^{\omega_1}]|0\rangle, \tag{76}$$

which can be written in matrix form as

$$(\mathbf{E} - \omega_1 \mathbf{S})\, \boldsymbol{\kappa}^{\omega_1} = \mathbf{V}^{\omega_1}, \tag{77}$$

where it has been used that $\hat{\kappa}^{\omega_1} = \hat{\mathbf{q}}^{\dagger} \boldsymbol{\kappa}^{\omega_1}$. The $\mathbf{E}$ matrix is defined through

$$\mathbf{E}\boldsymbol{\kappa}^{\omega_1} = -\langle 0|[\hat{\mathbf{q}}, [\hat{\kappa}^{\omega_1}, \hat{H}^{0}] + \hat{H}^{\omega_1}]|0\rangle, \tag{78}$$

the generalized overlap matrix is defined as

$$\mathbf{S} = \langle 0|[\hat{\mathbf{q}}, \hat{\mathbf{q}}^{\dagger}]|0\rangle, \tag{79}$$

and the perturbation vector is given by

$$\mathbf{V}^{\omega_1} = \langle 0|[\hat{\mathbf{q}}, \hat{V}^{\omega_1}]|0\rangle. \tag{80}$$

Having determined the first-order time-evolution parameters through Eq. (77), the linear response function $\langle\langle \hat{A}; \hat{V}^{\omega_1} \rangle\rangle_{\omega_1}$ for the property $\hat{A}$ perturbed by a periodic perturbation $\hat{V}^{\omega_1}$ with associated frequency ω_1 can be calculated as

$$\langle\langle \hat{A}; \hat{V}^{\omega_1} \rangle\rangle_{\omega_1} = \langle 0|[\hat{\kappa}^{\omega_1}, \hat{A}]|0\rangle = -\mathbf{A}^{\dagger} \boldsymbol{\kappa}^{\omega_1}. \tag{81}$$

Explicit contributions from the PE potential only enter the linear response function through the **E** matrix as

$$\mathbf{E}_{\mathrm{PE}}\boldsymbol{\kappa}^{\omega_1} = -\langle 0|[\hat{\mathbf{q}}, [\hat{\kappa}^{\omega_1}, \hat{v}^0_{\mathrm{PE}}] + \hat{v}^{\omega_1}_{\mathrm{PE}}]|0\rangle. \tag{82}$$

We define a new set of operators using one-index transformed integrals [15]

$$\hat{Q}^{\omega_1}_1 = [\hat{\kappa}^{\omega_1}, \hat{v}^0_{\mathrm{PE}}] = \hat{v}^0_{\mathrm{PE}}(\kappa^{\omega_1}) \tag{83}$$

$$\hat{Q}^{\omega_1}_2 = \hat{v}^{\omega_1}_{\mathrm{PE}} = -\sum_{s=1}^{S} \boldsymbol{\mu}^{\mathrm{ind}}_s(\tilde{\mathbf{F}}^{\omega_1})\hat{\mathbf{F}}^{(1)}_{s,\mathrm{el}}, \tag{84}$$

where the induced dipole moments are calculated using the transformed electric field $\tilde{\mathbf{F}}^{\omega_1}$ with elements evaluated according to

$$\tilde{\mathbf{F}}^{\omega_1}_s = \langle 0|[\hat{\kappa}^{\omega_1}, \hat{\mathbf{F}}^{(1)}_{s,\mathrm{el}}]|0\rangle = \langle 0|\hat{\mathbf{F}}^{(1)}_{s,\mathrm{el}}(\kappa^{\omega_1})|0\rangle. \tag{85}$$

Using the newly defined operators leads to a simplified expression for the PE contribution to the linearly transformed **E** matrix given by

$$\mathbf{E}_{\mathrm{PE}}\boldsymbol{\kappa}^{\omega_1} = -\langle 0|[\hat{\mathbf{q}}, \hat{Q}^{\omega_1}_1 + \hat{Q}^{\omega_1}_2]|0\rangle. \tag{86}$$

The $\hat{Q}^{\omega_1}_1$ operator gives the zeroth-order PE contribution to the linear response which corresponds to a static environment which does not respond to the applied perturbation, whereas the $\hat{Q}^{\omega_2}_2$ operator describes the dynamical response of the environment due to the perturbation. Here, it is important to note that this is the fully self-consistent many-body response without approximations, as opposed to other similar implementations [24, 25]. A common approximation corresponds to the use of a block-diagonal classical response matrix (Eq. (41)) in the response calculations, thus neglecting the off-diagonal interaction tensors, whereas we include the full classical response matrix in our model.

2.2.2. Quadratic response

The derivation of quadratic response proceeds analogous to the linear response case. Thus, we collect second-order terms from the BCH expansion of the Ehrenfest theorem as given in Eq. (74) and Fourier transform the resulting expression. In matrix form, this leads to

$$(\mathbf{E} - (\omega_1 + \omega_2)\mathbf{S})\boldsymbol{\kappa}^{\omega_1,\omega_2} = \mathbf{V}^{\omega_1,\omega_2}, \tag{87}$$

where the **E** matrix is defined through

$$\mathbf{E}\boldsymbol{\kappa}^{\omega_1,\omega_2} = \langle 0|[\hat{\mathbf{q}}, [\hat{H}^0, \hat{\kappa}^{\omega_1,\omega_2}] - {}^2\hat{H}^{\omega_1,\omega_2}]|0\rangle, \tag{88}$$

the **S** matrix is again the general overlap matrix, and the second-order perturbation vector $\mathbf{V}^{\omega_1,\omega_2}$ is defined as

$$\mathbf{V}^{\omega_1,\omega_2} = \hat{P}_{12}\Big(\langle 0|[\hat{\mathbf{q}},[\hat{\kappa}^{\omega_1},[\hat{\kappa}^{\omega_2},\hat{H}^0]] + 2[\hat{\kappa}^{\omega_1},\hat{H}^{\omega_2}+\hat{V}^{\omega_2}] + \omega_2[\hat{\mathbf{q}},[\hat{\kappa}^{\omega_1},\hat{\kappa}^{\omega_2}]] + {}^1\hat{H}^{\omega_1,\omega_2}]|0\rangle\Big). \tag{89}$$

We have used that the second-order perturbed density matrix elements (see Eq. (70)) can be separated into components due to first- and second-order parameters, respectively,

$$D_{pq}^{\omega_1,\omega_2} = {}^1D_{pq}^{\omega_1,\omega_2} + {}^2D_{pq}^{\omega_1,\omega_2}, \tag{90}$$

where

$${}^1D_{pq}^{\omega_1,\omega_2} = \hat{P}_{12}\langle 0|[\hat{\kappa}^{\omega_1},[\hat{\kappa}^{\omega_2},\hat{E}_{pq}]]|0\rangle \tag{91}$$

$${}^2D_{pq}^{\omega_1,\omega_2} = \langle 0|[\hat{\kappa}^{\omega_1,\omega_2},\hat{E}_{pq}]|0\rangle. \tag{92}$$

The separation of the density matrix elements allows the corresponding separation of the second-order Hamiltonian

$$\hat{H}^{\omega_1,\omega_2} = {}^1\hat{H}^{\omega_1,\omega_2} + {}^2\hat{H}^{\omega_1,\omega_2}, \tag{93}$$

where ${}^1\hat{H}^{\omega_1,\omega_2}$ depends on first-order parameters and ${}^2\hat{H}^{\omega_1,\omega_2}$ depends on second-order parameters. Instead of solving Eq. (87) for the second-order time-evolution parameters, we can solve the adjoint second-order linear response equation

$$\boldsymbol{\kappa}^{\mathbf{A}^\dagger}\big(\mathbf{E} - (\omega_1+\omega_2)\mathbf{S}\big) = \mathbf{A}^\dagger. \tag{94}$$

The first-order parameters are determined by solving two first-order linear response equations

$$\big(\mathbf{E} - \omega_i\mathbf{S}\big)\boldsymbol{\kappa}^{\omega_i} = \mathbf{V}^{\omega_i}, \tag{95}$$

where $i = 1$ or 2. The quadratic response function $\langle\langle \hat{A}; \hat{V}^{\omega_1}, \hat{V}^{\omega_2}\rangle\rangle_{\omega_1,\omega_2}$ for the property $\hat{A}$ perturbed by two periodic perturbations $\hat{V}^{\omega_1}$ and $\hat{V}^{\omega_2}$ with associated frequencies ω_1 and ω_2, respectively, is given by

$$\langle\langle \hat{A}; \hat{V}^{\omega_1}, \hat{V}^{\omega_2}\rangle\rangle_{\omega_1,\omega_2} = \langle 0|[\hat{\kappa}^{\omega_1,\omega_2},\hat{A}]|0\rangle + \hat{P}_{12}\langle 0|[\hat{\kappa}^{\omega_1},[\hat{\kappa}^{\omega_2},\hat{A}]]|0\rangle. \tag{96}$$

The explicit PE contributions to the quadratic response function enter the **E** matrix (Eq. (88)) and the $\mathbf{V}^{\omega_1,\omega_2}$ vector (Eq. (89)). Contributions that appear

in the **E** matrix are analogous to the linear response case, that is,

$$\mathbf{E}_{\mathrm{PE}}\boldsymbol{\kappa}^{\omega_1,\omega_2} = -\langle 0|[\hat{\mathbf{q}}, \hat{Q}_1^{\omega_1,\omega_2} + \hat{Q}_2^{\omega_1,\omega_2}]|0\rangle, \tag{97}$$

where

$$\hat{Q}_1^{\omega_1,\omega_2} = [\hat{\kappa}^{\omega_1,\omega_2}, \hat{v}_{\mathrm{PE}}^0] = \hat{v}_{\mathrm{PE}}^0(\kappa^{\omega_1,\omega_2}) \tag{98}$$

$$\hat{Q}_2^{\omega_1,\omega_2} = {}^2\hat{v}_{\mathrm{PE}}^{\omega_1,\omega_2} = -\sum_{s=1}^{S} \boldsymbol{\mu}_s^{\mathrm{ind}}({}^2\tilde{\mathbf{F}}^{\omega_1,\omega_2})\hat{\mathbf{F}}_{s,\mathrm{el}}^{(1)}. \tag{99}$$

The induced dipoles in $\hat{Q}_2^{\omega_1,\omega_2}$ are calculated using the transformed electric field with elements given by

$${}^2\tilde{\mathbf{F}}_s^{\omega_1,\omega_2} = \langle 0|[\hat{\kappa}^{\omega_1,\omega_2}, \hat{\mathbf{F}}_{s,\mathrm{el}}^{(1)}]|0\rangle = \langle 0|\hat{\mathbf{F}}_{s,\mathrm{el}}^{(1)}(\kappa^{\omega_1,\omega_2})|0\rangle. \tag{100}$$

The contributions to the perturbation vector are

$$\mathbf{V}_{\mathrm{PE}}^{\omega_1,\omega_2} = \langle 0|[\hat{\mathbf{q}}, \hat{Q}_3^{\omega_1,\omega_2} + \hat{Q}_4^{\omega_1,\omega_2} + \hat{Q}_5^{\omega_1,\omega_2}]|0\rangle, \tag{101}$$

where we have used new operators defined by

$$\hat{Q}_3^{\omega_1,\omega_2} = \hat{P}_{12}[\hat{\kappa}^{\omega_1}, [\hat{\kappa}^{\omega_2}, \hat{v}_{\mathrm{PE}}^0]] = \hat{P}_{12}\hat{v}_{\mathrm{PE}}^0(\kappa^{\omega_2}, \kappa^{\omega_1}) \tag{102}$$

$$\begin{aligned}\hat{Q}_4^{\omega_1,\omega_2} &= 2\hat{P}_{12}[\hat{\kappa}^{\omega_1}, \hat{v}_{\mathrm{PE}}^{\omega_2}] \\ &= -2\hat{P}_{12}\sum_{s=1}^{S} \boldsymbol{\mu}_s^{\mathrm{ind}}(\tilde{\mathbf{F}}^{\omega_2})[\hat{\kappa}^{\omega_1}, \hat{\mathbf{F}}_{s,\mathrm{el}}^{(1)}] \\ &= -2\hat{P}_{12}\sum_{s=1}^{S} \boldsymbol{\mu}_s^{\mathrm{ind}}(\tilde{\mathbf{F}}^{\omega_2})\hat{\mathbf{F}}_{s,\mathrm{el}}^{(1)}(\kappa^{\omega_1})\end{aligned} \tag{103}$$

$$\begin{aligned}\hat{Q}_5^{\omega_1,\omega_2} &= \hat{P}_{12}\,{}^1\hat{v}_{\mathrm{PE}}^{\omega_1,\omega_2} \\ &= -\hat{P}_{12}\sum_{s=1}^{S} \boldsymbol{\mu}_s^{\mathrm{ind}}({}^1\tilde{\mathbf{F}}^{\omega_1,\omega_2})\hat{\mathbf{F}}_{s,\mathrm{el}}^{(1)}.\end{aligned} \tag{104}$$

The perturbed electric field $\tilde{\mathbf{F}}^{\omega_2}$ is defined analogous to Eq. (85), and ${}^1\tilde{\mathbf{F}}^{\omega_1,\omega_2}$ is defined through

$${}^1\tilde{\mathbf{F}}_s^{\omega_1,\omega_2} = \langle 0|[\hat{\kappa}^{\omega_1}, [\hat{\kappa}^{\omega_2}, \hat{\mathbf{F}}_{s,\mathrm{el}}^{(1)}]]|0\rangle = \hat{\mathbf{F}}_{s,\mathrm{el}}^{(1)}(\kappa^{\omega_2}, \kappa^{\omega_1}). \tag{105}$$

The zeroth-order terms, that is, $\hat{Q}_1^{\omega_1,\omega_2}$ and $\hat{Q}_3^{\omega_1,\omega_2}$, give the contributions to the response function that arise from a static environment analogous to the linear response case. All the other contributions, that is, $\hat{Q}_2^{\omega_1,\omega_2}$, $\hat{Q}_4^{\omega_1,\omega_2}$, and $\hat{Q}_5^{\omega_1,\omega_2}$, account for the dynamical response of the environment due to the periodic perturbations.

2.2.3. Cubic response

The derivation of cubic response is analogous to what we have seen so far. We use the BCH expansion of the Ehrenfest theorem but now collect terms that are third order in the perturbation. The resulting matrix equation is

$$\big(\mathbf{E} - (\omega_1 + \omega_2 + \omega_3)\mathbf{S}\big)\boldsymbol{\kappa}^{\omega_1,\omega_2,\omega_3} = \mathbf{V}^{\omega_1,\omega_2,\omega_3}, \tag{106}$$

where $\mathbf{S}$ is the general overlap matrix, the $\mathbf{E}$ matrix is defined through

$$\mathbf{E}\boldsymbol{\kappa}^{\omega_1,\omega_2,\omega_3} = \langle 0|[\hat{\mathbf{q}}, [\hat{H}^0, \hat{\kappa}^{\omega_1,\omega_2,\omega_3}] - {}^2\hat{H}^{\omega_1,\omega_2,\omega_3}]|0\rangle, \tag{107}$$

and the third-order perturbation vector is given by

$$\begin{aligned}
\mathbf{V}^{\omega_1,\omega_2,\omega_3} = \hat{P}_{123}\langle 0|[\hat{\mathbf{q}}, [\hat{\kappa}^{\omega_1}, [\hat{\kappa}^{\omega_2}, [\hat{\kappa}^{\omega_3}, \hat{H}^0]]] + \frac{3}{2}[\hat{\kappa}^{\omega_1}, [\hat{\kappa}^{\omega_2,\omega_3}, \hat{H}^0]] \\
+ \frac{3}{2}[\hat{\kappa}^{\omega_1,\omega_2}, [\hat{\kappa}^{\omega_3}, \hat{H}^0]] + 3[\hat{\kappa}^{\omega_1}, [\hat{\kappa}^{\omega_2}, \hat{H}^{\omega_3} + \hat{V}^{\omega_3}]] \\
+ 3[\hat{\kappa}^{\omega_1}, \hat{H}^{\omega_2,\omega_3}] + 3[\hat{\kappa}^{\omega_1,\omega_2}, \hat{H}^{\omega_3} + \hat{V}^{\omega_3}] \\
+ \omega_3[\hat{\kappa}^{\omega_1}, [\hat{\kappa}^{\omega_2}, \hat{\kappa}^{\omega_3}]] + \frac{3}{2}(\omega_2 + \omega_3)[\hat{\kappa}^{\omega_1}, \hat{\kappa}^{\omega_2,\omega_3}] \\
+ \frac{3}{2}\omega_3[\hat{\kappa}^{\omega_1,\omega_2}, \hat{\kappa}^{\omega_3}] + {}^1\hat{H}^{\omega_1,\omega_2,\omega_3}]|0\rangle.
\end{aligned} \tag{108}$$

Here, we have also separated the perturbed density matrix into terms that depend on first- and second-order, and third-order parameters, respectively, as

$$D_{pq}^{\omega_1,\omega_2,\omega_3} = {}^1D_{pq}^{\omega_1,\omega_2,\omega_3} + {}^2D_{pq}^{\omega_1,\omega_2,\omega_3} \tag{109}$$

where

$$\begin{aligned}
{}^1D_{pq}^{\omega_1,\omega_2,\omega_3} = \hat{P}_{123}\langle 0|\tfrac{3}{2}[\hat{\kappa}^{\omega_1}, [\hat{\kappa}^{\omega_2,\omega_3}, \hat{E}_{pq}]] + \tfrac{3}{2}[\hat{\kappa}^{\omega_1,\omega_2}, [\hat{\kappa}^{\omega_3}, \hat{E}_{pq}]] \\
+ [\hat{\kappa}^{\omega_1}, [\hat{\kappa}^{\omega_2}, [\hat{\kappa}^{\omega_3}, \hat{E}_{pq}]]]|0\rangle
\end{aligned} \tag{110}$$

$${}^2D_{pq}^{\omega_1,\omega_2,\omega_3} = \langle 0|[\hat{\kappa}^{\omega_1,\omega_2,\omega_3}, \hat{E}_{pq}]|0\rangle. \tag{111}$$

Thus allowing us to write the third-order Hamiltonian as

$$\hat{H}^{\omega_1,\omega_2,\omega_3} = {}^1\hat{H}^{\omega_1,\omega_2,\omega_3} + {}^2\hat{H}^{\omega_1,\omega_2,\omega_3} \tag{112}$$

where ${}^1\hat{H}^{\omega_1,\omega_2,\omega_3}$ depends on first- and second-order parameters and ${}^2\hat{H}^{\omega_1,\omega_2,\omega_3}$ only depends on third-order parameters. The first- and second-order variational parameters are determined by solving three first-order linear response equations

$$\big(\mathbf{E} - \omega_i \mathbf{S}\big)\boldsymbol{\kappa}^{\omega_i} = \mathbf{V}^{\omega_i}, \tag{113}$$

where $i = 1$, 2, or 3, and three second-order linear response equations

$$\big(\mathbf{E} - (\omega_i + \omega_j)\mathbf{S}\big)\boldsymbol{\kappa}^{\omega_i,\omega_j} = \mathbf{V}^{\omega_i,\omega_j} \tag{114}$$

where $j > i$ and $i, j = 1$, 2, or 3, or the adjoints (Eq. (94)) of them. The third-order parameters are determined by the adjoint third-order linear response equation

$$\boldsymbol{\kappa}^{\mathbf{A}^\dagger}\big(\mathbf{E} - (\omega_1 + \omega_2 + \omega_3)\mathbf{S}\big) = \mathbf{A}^\dagger. \tag{115}$$

The cubic response function $\langle\langle \hat{A}; \hat{V}^{\omega_1}, \hat{V}^{\omega_2}, \hat{V}^{\omega_3} \rangle\rangle_{\omega_1,\omega_2,\omega_3}$ for the property $\hat{A}$ perturbed by the periodic perturbations $\hat{V}^{\omega_1}$, $\hat{V}^{\omega_2}$, and $\hat{V}^{\omega_3}$ with associated frequencies ω_1, ω_2, and ω_3, respectively, is given by

$$\begin{aligned}
\langle\langle \hat{A}; \hat{V}^{\omega_1}, \hat{V}^{\omega_2}, \hat{V}^{\omega_3} \rangle\rangle_{\omega_1,\omega_2,\omega_3} = {} & \langle 0|[\hat{\kappa}^{\omega_1,\omega_2,\omega_3}, \hat{A}]|0\rangle \\
& + \frac{3}{2}\hat{P}_{123}\langle 0|[\hat{\kappa}^{\omega_1}, [\hat{\kappa}^{\omega_2,\omega_3}, \hat{A}]]|0\rangle \\
& + \frac{3}{2}\hat{P}_{123}\langle 0|[\hat{\kappa}^{\omega_1,\omega_2}, [\hat{\kappa}^{\omega_3}, \hat{A}]]|0\rangle \\
& + \hat{P}_{123}\langle 0|[\hat{\kappa}^{\omega_1}, [\hat{\kappa}^{\omega_2}, [\hat{\kappa}^{\omega_3}, \hat{A}]]]|0\rangle.
\end{aligned} \tag{116}$$

We will now detail the explicit contributions that are due to the PE potential to the cubic response function, which enter through the $\mathbf{E}$ matrix and the $\mathbf{V}^{\omega_1,\omega_2,\omega_3}$ vector. The contributions to the $\mathbf{E}$ matrix are defined through

$$\mathbf{E}_{\mathrm{PE}}\boldsymbol{\kappa}^{\omega_1,\omega_2,\omega_3} = -\langle 0|[\hat{\mathbf{q}}, \hat{Q}_1^{\omega_1,\omega_2,\omega_3} + \hat{Q}_2^{\omega_1,\omega_2,\omega_3}|0\rangle, \tag{117}$$

where the $\hat{Q}_1^{\omega_1,\omega_2,\omega_3}$ operator contains the zeroth-order PE potential operator and is defined as

$$\hat{Q}_1^{\omega_1,\omega_2,\omega_3} = [\hat{\kappa}^{\omega_1,\omega_2,\omega_3}, \hat{v}^0_{\mathrm{PE}}] = \hat{v}^0_{\mathrm{PE}}(\boldsymbol{\kappa}^{\omega_1,\omega_2,\omega_3}), \tag{118}$$

and the $\hat{Q}_2^{\omega_1,\omega_2,\omega_3}$ operator contains the part of the third-order PE potential operator that only depends on the third-order parameters and is defined as

$$\hat{Q}_2^{\omega_1,\omega_2,\omega_3} = {}^2\hat{v}_{\mathrm{PE}}^{\omega_1,\omega_2,\omega_3} = -\sum_{s=1}^{S} \boldsymbol{\mu}_s^{\mathrm{ind}}({}^2\tilde{\mathbf{F}}^{\omega_1,\omega_2,\omega_3})\hat{\mathbf{F}}_{s,\mathrm{el}}^{(1)}. \tag{119}$$

The induced dipoles in $\hat{Q}_2^{\omega_1,\omega_2,\omega_3}$ depend on the transformed electric field ${}^2\tilde{\mathbf{F}}^{\omega_1,\omega_2,\omega_3}$ that is given through

$${}^2\tilde{\mathbf{F}}_s^{\omega_1,\omega_2,\omega_3} = \langle 0|[\hat{\kappa}^{\omega_1,\omega_2,\omega_3}, \hat{\mathbf{F}}_{s,\mathrm{el}}^{(1)}]|0\rangle = \langle 0|\hat{\mathbf{F}}_{s,\mathrm{el}}^{(1)}(\boldsymbol{\kappa}^{\omega_1,\omega_2,\omega_3})|0\rangle. \tag{120}$$

The contributions to the perturbation vector are defined as

$$\begin{aligned}\mathbf{V}_{\mathrm{PE}}^{\omega_1,\omega_2,\omega_3} = \langle 0|[\hat{\mathbf{q}}, \hat{Q}_3^{\omega_1,\omega_2,\omega_3} + \hat{Q}_4^{\omega_1,\omega_2,\omega_3} + \hat{Q}_5^{\omega_1,\omega_2,\omega_3} + \hat{Q}_6^{\omega_1,\omega_2,\omega_3} \\ + \hat{Q}_7^{\omega_1,\omega_2,\omega_3} + \hat{Q}_8^{\omega_1,\omega_2,\omega_3} + \hat{Q}_9^{\omega_1,\omega_2,\omega_3}]|0\rangle,\end{aligned} \tag{121}$$

where we again define new operators. Here, the $\hat{Q}_3^{\omega_1,\omega_2,\omega_3}$, $\hat{Q}_4^{\omega_1,\omega_2,\omega_3}$, and $\hat{Q}_5^{\omega_1,\omega_2,\omega_3}$ operators contain the zeroth-order PE potential operator and are defined as

$$\hat{Q}_3^{\omega_1,\omega_2,\omega_3} = \hat{P}_{123}[\hat{\kappa}^{\omega_1}, [\hat{\kappa}^{\omega_2}, [\hat{\kappa}^{\omega_3}, \hat{v}_{\mathrm{PE}}^0]]] = \hat{P}_{123}\hat{v}_{\mathrm{PE}}^0(\boldsymbol{\kappa}^{\omega_3}, \boldsymbol{\kappa}^{\omega_2}, \boldsymbol{\kappa}^{\omega_1}) \tag{122}$$

$$\hat{Q}_4^{\omega_1,\omega_2,\omega_3} = \frac{3}{2}\hat{P}_{123}[\hat{\kappa}^{\omega_1}, [\hat{\kappa}^{\omega_2,\omega_3}, \hat{v}_{\mathrm{PE}}^0]] = \frac{3}{2}\hat{P}_{123}\hat{v}_{\mathrm{PE}}^0(\boldsymbol{\kappa}^{\omega_2,\omega_3}, \boldsymbol{\kappa}^{\omega_1}) \tag{123}$$

$$\hat{Q}_5^{\omega_1,\omega_2,\omega_3} = \frac{3}{2}\hat{P}_{123}[\hat{\kappa}^{\omega_1,\omega_2}, [\hat{\kappa}^{\omega_3}, \hat{v}_{\mathrm{PE}}^0]] = \frac{3}{2}\hat{P}_{123}\hat{v}_{\mathrm{PE}}^0(\boldsymbol{\kappa}^{\omega_3}, \boldsymbol{\kappa}^{\omega_1,\omega_2}), \tag{124}$$

whereas the $\hat{Q}_6^{\omega_1,\omega_2,\omega_3}$ and $\hat{Q}_7^{\omega_1,\omega_2,\omega_3}$ operators contain first-order PE potential operators and are defined as

$$\begin{aligned}\hat{Q}_6^{\omega_1,\omega_2,\omega_3} &= 3\hat{P}_{123}[\hat{\kappa}^{\omega_1}, [\hat{\kappa}^{\omega_2}, \hat{v}_{\mathrm{PE}}^{\omega_3}]] \\ &= -3\hat{P}_{123}\sum_{s=1}^{S} \boldsymbol{\mu}_s^{\mathrm{ind}}(\tilde{\mathbf{F}}^{\omega_3})\hat{\mathbf{F}}_{s,\mathrm{el}}^{(1)}(\boldsymbol{\kappa}^{\omega_2}, \boldsymbol{\kappa}^{\omega_1}),\end{aligned} \tag{125}$$

$$\hat{Q}_7^{\omega_1,\omega_2,\omega_3} = 3\hat{P}_{123}[\hat{\kappa}^{\omega_1,\omega_2}, \hat{v}_{\mathrm{PE}}^{\omega_3}] = -3\hat{P}_{123}\sum_{s=1}^{S} \boldsymbol{\mu}_s^{\mathrm{ind}}(\tilde{\mathbf{F}}^{\omega_3})\hat{\mathbf{F}}_{s,\mathrm{el}}^{(1)}(\boldsymbol{\kappa}^{\omega_1,\omega_2}). \tag{126}$$

The transformed electric field $\tilde{\mathbf{F}}^{\omega_3}$ is defined through

$$\tilde{\mathbf{F}}_s^{\omega_3} = \langle 0|[\hat{\kappa}^{\omega_3}, \hat{\mathbf{F}}_{s,\mathrm{el}}^{(1)}]|0\rangle = \langle 0|\hat{\mathbf{F}}_{s,\mathrm{el}}^{(1)}(\boldsymbol{\kappa}^{\omega_3})|0\rangle. \tag{127}$$

The $\hat{Q}_8^{\omega_1,\omega_2,\omega_3}$ operator contains a second-order PE potential operator and is defined as

$$\hat{Q}_8^{\omega_1,\omega_2,\omega_3} = 3\hat{P}_{123}[\hat{\kappa}^{\omega_1}, \hat{v}_{\mathrm{PE}}^{\omega_2,\omega_3}] = -3\hat{P}_{123}\sum_{s=1}^{S} \boldsymbol{\mu}_s^{\mathrm{ind}}(\tilde{\mathbf{F}}^{\omega_2,\omega_3})\hat{\mathbf{F}}_{s,\mathrm{el}}^{(1)}(\boldsymbol{\kappa}^{\omega_1}), \tag{128}$$

where the induced dipoles depend on the electric field from the second-order electron density (Eq. (90)). The transformed electric field $\tilde{\mathbf{F}}^{\omega_2,\omega_3}$ is therefore given through

$$\begin{aligned}\tilde{\mathbf{F}}_s^{\omega_2,\omega_3} &= \langle 0|[\hat{\kappa}^{\omega_2,\omega_3}, \hat{\mathbf{F}}_{s,\mathrm{el}}^{(1)}] + \hat{P}_{23}[\hat{\kappa}^{\omega_2}, [\hat{\kappa}^{\omega_3}, \hat{\mathbf{F}}_{s,\mathrm{el}}^{(1)}]]|0\rangle \\ &= \langle 0|\hat{\mathbf{F}}_{s,\mathrm{el}}^{(1)}(\boldsymbol{\kappa}^{\omega_2,\omega_3}) + \hat{P}_{23}\hat{\mathbf{F}}_{s,\mathrm{el}}^{(1)}(\boldsymbol{\kappa}^{\omega_3}, \boldsymbol{\kappa}^{\omega_2})|0\rangle. \end{aligned} \tag{129}$$

Finally, the $\hat{Q}_9^{\omega_1,\omega_2,\omega_3}$ operator, which contains the part of the third-order PE potential operator and depends on lower order variational parameters, is defined as

$$\hat{Q}_9^{\omega_1,\omega_2,\omega_3} = \hat{P}_{123}\,{}^1\hat{v}_{\mathrm{PE}}^{\omega_1,\omega_2,\omega_3} = -\hat{P}_{123}\sum_{s=1}^{S} \boldsymbol{\mu}_s^{\mathrm{ind}}({}^1\tilde{\mathbf{F}}^{\omega_1,\omega_2,\omega_3})\hat{\mathbf{F}}_{s,\mathrm{el}}^{(1)}. \tag{130}$$

Here, the induced dipoles depend on the electric field from the part of the third-order electron density which depends on lower order parameters (Eq. (110)). The transformed electric field ${}^1\tilde{\mathbf{F}}^{\omega_1,\omega_2,\omega_3}$ is, thus, defined through

$$\begin{aligned}{}^1\tilde{\mathbf{F}}_s^{\omega_1,\omega_2,\omega_3} &= \langle 0|\frac{3}{2}[\hat{\kappa}^{\omega_1}, [\hat{\kappa}^{\omega_2,\omega_3}, \hat{\mathbf{F}}_{s,\mathrm{el}}^{(1)}]] + \frac{3}{2}[\hat{\kappa}^{\omega_1,\omega_2}, [\hat{\kappa}^{\omega_3}, \hat{\mathbf{F}}_{s,\mathrm{el}}^{(1)}]] \\ &\quad + [\hat{\kappa}^{\omega_1}, [\hat{\kappa}^{\omega_2}, [\hat{\kappa}^{\omega_3}, \hat{\mathbf{F}}_{s,\mathrm{el}}^{(1)}]]]|0\rangle \\ &= \langle 0|\frac{3}{2}\hat{\mathbf{F}}_{s,\mathrm{el}}^{(1)}(\boldsymbol{\kappa}^{\omega_2,\omega_3}, \boldsymbol{\kappa}^{\omega_1}) + \frac{3}{2}\hat{\mathbf{F}}_{s,\mathrm{el}}^{(1)}(\boldsymbol{\kappa}^{\omega_3}, \boldsymbol{\kappa}^{\omega_1,\omega_2}) \\ &\quad + \hat{\mathbf{F}}_{s,\mathrm{el}}^{(1)}(\boldsymbol{\kappa}^{\omega_3}, \boldsymbol{\kappa}^{\omega_2}, \boldsymbol{\kappa}^{\omega_1})|0\rangle. \end{aligned} \tag{131}$$

Considerations regarding the effect that the operators have, with respect to the response in the environment, are analogous to the linear and quadratic response, that is, zeroth-order terms correspond to a static environment, whereas higher-order terms account for dynamic response in the environment.

2.3. Calculation of nuclear magnetic shielding tensors for embedded molecules

Nuclear magnetic resonance (NMR) is one of the most important site-specific and sensitive probes for electronic environments and hence for molecular

structure determination. In this section, we will briefly outline the theory related to the calculation of NMR shielding constants within the polarizable embedding approach. The nuclear magnetic shielding tensor $\boldsymbol{\sigma}^N$ for nucleus N is defined as the second-order response of the electronic energy to an external magnetic induction ($\mathbf{B}$) and a nuclear magnetic moment ($\mathbf{m}_N$). In the atomic orbital (AO) basis, the expression becomes (see e.g., the discussion in Refs. [26, 27])

$$\begin{aligned}\sigma_{ij}^N &= 1 + \left[\frac{\mathrm{d}^2 E}{\mathrm{d}B_i \mathrm{d}m_{N_j}}\right]_{B=m_{N_j}=0} \\ &= 1 + \sum_{\mu\nu} D_{\mu\nu} \frac{\partial^2 h_{\mu\nu}}{\partial B_i \partial m_{N_j}} + \sum_{\mu\nu} \frac{\partial D_{\mu\nu}}{\partial B_i} \frac{\partial h_{\mu\nu}}{\partial m_{N_j}},\end{aligned} \tag{132}$$

where $D_{\mu\nu}$ is an element of the density matrix in the AO basis and $h_{\mu\nu}$ is a matrix element of the effective one-electron Hamiltonian. In our implementation of the nuclear magnetic shielding tensors, the second term in Eq. (132) (the paramagnetic contribution) is determined by solving a set of PE-DFT response equations [23, 24, 28] for the three components of the magnetic induction. In order to ensure origin-independent results for the nuclear magnetic shielding constants, we use gauge-including atomic orbitals (GIAOs) [29–32]—that is, the AO basis functions depend explicitly on the magnetic induction through

$$\chi_\mu(\mathbf{B}) = \exp\left(\frac{-i}{2}(\mathbf{B} \times \mathbf{R}_\mu) \cdot \mathbf{r}\right) \chi_\mu(0), \tag{133}$$

where $\mathbf{R}_\mu$ is the vector giving the position of the nucleus to which the field-dependent basis function is attached relative to the global gauge origin, and $\chi_\mu(0)$ indicates a conventional AO basis function not depending on $\mathbf{B}$. Equation (132) applies both to the case of a molecule in vacuum and within an environment. The (polarizable) environment contributes both through the density matrix, which is obtained self-consistently including the perturbation from the surroundings, *and* through the derivative of the density matrix (or the response vectors in our context) with respect to the magnetic induction, that is, both terms in Eq. (132) contain the effect of the environment [33].

The first derivative of the density matrix with respect to the magnetic induction is obtained by solving the coupled-perturbed Kohn–Sham (CPKS) equations to which the first derivative of the effective Kohn–Sham operator with respect to the magnetic induction contributes. We refer to Ref. [34] for a discussion of this and related issues regarding the calculation of nuclear magnetic shielding constants using HF or DFT methods. In our context, we need to solve the response equations corresponding to the perturbation from

the magnetic induction. Due to the use of GIAOs, specific corrections arising from the effective operator describing the environment effects will appear. In the following, we will focus on these contributions [35].

In the field-dependent AO basis, an element of the PE potential operator becomes

$$v_{\mathrm{PE},\mu\nu} = \sum_{s=1}^{S}\sum_{|k|=0}^{K}\frac{(-1)^{|k|}}{k!}Q_s^{(k)}t_{s,\mu\nu}^{(k)} - \sum_{s=1}^{S}\boldsymbol{\mu}_s^{\mathrm{ind}}(\mathbf{F}_{\mathrm{tot}})\mathbf{t}_{s,\mu\nu}^{(1)}, \tag{134}$$

where the integrals are taken over the interaction tensors used in all cases of the field-dependent AOs. The first derivative of the PE potential operator with respect to the magnetic induction may be written in the same form as $\hat{v}_{\mathrm{PE}}$ but with modified integrals [35]

$$\frac{dv_{\mathrm{PE},\mu\nu}}{dB_i} = \sum_{s=1}^{S}\sum_{|k|=0}^{K}\frac{(-1)^{|k|}}{k!}Q_s^{(k)}t_{s,\mu\nu,B_i}^{(k)} - \sum_{s=1}^{S}\boldsymbol{\mu}_s^{\mathrm{ind}}(\mathbf{F}_{\mathrm{tot}})\mathbf{t}_{s,\mu\nu,B_i}^{(1)}. \tag{135}$$

In Eq. (135), $t_{s,\mu\nu,B_i}^{(k)}$ is defined as

$$t_{s,\mu\nu,B_i}^{(k)} = \langle\chi_\mu^{B_i}|T_s^{(k)}(\mathbf{r})|\chi_\nu\rangle + \langle\chi_\mu|T_s^{(k)}(\mathbf{r})|\chi_\nu^{B_i}\rangle, \tag{136}$$

where the superscript on the atomic orbitals indicates differentiation of the relevant quantity. Such integrals may be evaluated, following the notation introduced in Refs. [28, 36], by use of the general expression for the first derivative of an arbitrary nondifferential operator (I) that does not depend on the magnetic induction

$$(I_{\mu\nu,\mathbf{B}})_{\mathbf{B}=0} = \frac{i}{2}Q_{MN}\langle\chi_\mu|\mathbf{r}I|\chi_\nu\rangle, \tag{137}$$

where we have located χ_μ at $\mathbf{R}_M$ and χ_ν at $\mathbf{R}_N$, and where Q_{MN} is defined as

$$Q_{MN} = \begin{pmatrix} 0 & -Z_{MN} & Y_{MN} \\ Z_{MN} & 0 & -X_{MN} \\ -Y_{MN} & X_{MN} & 0 \end{pmatrix}. \tag{138}$$

Finally, combining Eqs. (135 and 137) enables us to derive an equation for calculating the required derivatives of the environmental contributions because of the use of GIAOs.

3. RESULTS AND DISCUSSION

In the following, we will review a few selected applications related to the PE-DFT approach. Here, the focus will be on solute–solvent systems, although

the PE scheme is generally applicable to any confined molecular system such as for example photoactive proteins [7]. We will begin by discussing the general accuracy of the embedding potential.

3.1. The accuracy of the embedding potential: A hierarchy of force fields

To model the effects of the solvent molecules in a solute–solvent system, we use PE potentials based on a hierarchy of force fields as defined by the LoProp approach [37], which is a scheme for calculating localized multipoles and polarizabilities. The derived force fields are based on B3LYP/aug-cc-pVTZ and have been obtained from the Molcas program [38]. The force fields are classified as MXPY where X denotes the highest order of the multipole moments and Y indicates whether it includes isotropic ($Y = 1$) or anisotropic ($Y = 2$) polarizabilities. These parameters are attributed to the atomic sites of the solvent molecules, which, in the present context, will be water. In addition to the MXPY force fields, we also define a force field denoted M2P2BM, which includes multipoles up to quadrupoles and anisotropic polarizabilities assigned to both atomic sites and bond midpoints. The above discussed force fields all include polarization effects explicitly. However, to compare with force fields where polarization is included implicitly, a series of force fields using the PCM model [19], which we denote MXPCM, is also derived and discussed. In this case, the induction effects are incorporated implicitly into the multipole moments. Finally, we have, for comparison, also included results based on the use of the conventional Ahlström [39] force field (a simplified polarizable force field) and the standard nonpolarizable TIP3P force field due to Jorgensen [40].

The quality of the force fields is assessed by comparing the molecular electrostatic potentials, in the vicinity of the molecule, based on the force field and quantum chemical reference calculations. The electrostatic potential is the most suitable observable for such a comparison since it enters directly in the PE potential operator. To probe the electrostatic potential, a grid was constructed around the water molecule, see Ref. [6] for details concerning the construction of this grid. The electrostatic potential, due to the multipoles, at the ath grid point was calculated according to

$$\varphi_a = \sum_{s=1}^{S} \sum_{|k|=0}^{K} \frac{(-1)^{|k|}}{k!} T_{as}^{(k)} Q_s^{(k)}, \tag{139}$$

where the summation is over all multipole expansion centers in the molecule and all multipoles. The QM electrostatic potential at the ath grid point is the expectation value of the $|\mathbf{r}_a - \mathbf{r}|^{-1}$ operator plus the nuclear contribution. The B3LYP exchange-correlation functional and the aug-cc-pVTZ basis set, that is, the same method used to derive the LoProp force fields, were used to evaluate the QM reference electrostatic potential. The analysis is then performed

in terms of the root mean square deviation (RMSD)

$$\mathrm{RMSD} = \sqrt{\frac{1}{N}\sum_{a}\left(\varphi_a - \varphi_a^{\mathrm{QM}}\right)^2}, \tag{140}$$

where N is the number of the grid points. Following similar strategies, it is possible to probe the quality of the polarizabilities. However, for the polarizabilities, it is necessary to apply an external homogeneous electric field in the calculation of the electrostatic potential. This field will give rise to induced dipoles, which in turn creates an electrostatic potential around the molecule. Two calculations are then performed at the B3LYP/aug-cc-pVTZ level: one with and another without the external electric field. The QM reference is then obtained by subtracting the electrostatic potential in vacuum from that in the external field at every grid point.

In Figure 3.1, we present the RMSD obtained by a comparison between the molecular electrostatic potential due to multipole moments taken from the considered force fields and the quantum mechanically computed potential for different distances from the molecular van der Waals surface. From Figure 3.1, it is clearly demonstrated that the multipole expansion is appropriate at large distances from the molecule and that higher order multipoles are mandatory to consider when the molecular potential close to the

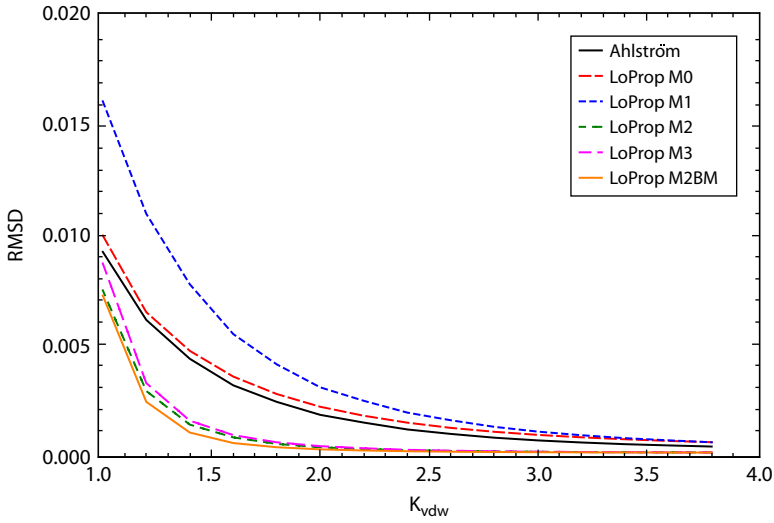

Figure 3.1 The RMSD of the molecular electrostatic potential due to the multipoles of a water molecule as a function of the distance from the molecular van der Waals surface. The distance from the surface is given as the factor scaling the van der Waals radii. The RMSD is in a.u. Results from Ref. [6].

molecule is probed. Quadrupole moments have a very pronounced effect and improve the molecular electrostatic potential considerably, as it was also found in Ref. [41]. On the other hand, the octopole moments contribute little to the accuracy of the electrostatic potential. The atomic point charges in the Ahlström force field are constructed so as to implicitly include higher order multipoles. However, it is evident from Figure 3.1 that the improvement is negligible compared with the M0 force field and cannot match the performance of the M2 force field. We see that the LoProp force field that includes multipoles at bond midpoints (M2BM) offers minor improvement as well. We also inspected the M3BM force field, and additional octopoles placed at bond midpoints were found to provide virtually no improvement.

Similarly, in Figure 3.2, we compare the induced changes in the electrostatic potentials due to an external electric field. From this we observe that the distributed isotropic polarizabilities in the LoProp force field lead to a more accurate account of the polarization of the electrostatic potential as compared to the single molecular isotropic polarizability assigned to the oxygen site of the water molecule in the Ahlström force field. Further improvement, though not that pronounced, is achieved by using the anisotropic polarizabilities. However, a larger difference in other molecules with a higher degree of anisotropy than the water molecule could be expected. We note that the RMSD in the case of induced dipoles is smaller by at least an order of magnitude than that due to the multipoles. This indicates

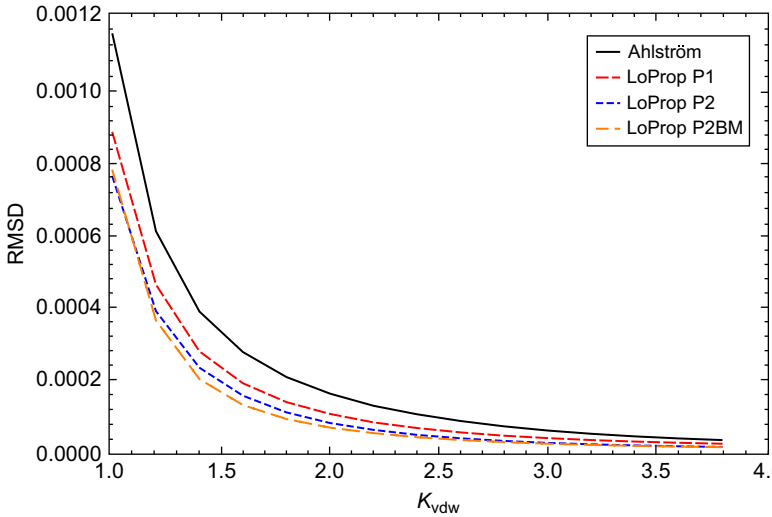

Figure 3.2 The RMSD of the molecular electrostatic potential due to the induced dipole moments of a water molecule as a function of the distance from the molecular van der Waals surface. The distance from the surface is given as the factor scaling the van der Waals radii. The RMSD is in a.u. Results from Ref. [6].

that the specific description of the polarization is not as important as an accurate account of the electrostatics.

3.2. Excitation energies

In this section, we examine the effects from a water solvent on the excitation energies of the solute molecule, acetone, using the PE-DFT method in combination with the embedding potentials assessed in Section 3.1 More specifically, we investigate the behavior of the solvent-induced shifts of the excitation energies as we vary the complexity of the force field used in the PE-DFT calculations. The QM region is restricted to contain only the solute molecule, and we thereby only include electrostatic and induction effects in the calculated shifts. The PE-DFT results for the shift of the excitation energies in acetone are the statistical averages over 120 molecular configurations extracted from a molecular dynamics simulation [6]. A spherical cutoff radius equal to 12 Å based on the distance between the center of masses of the solute and solvent molecules was used for every configuration. The calculations are furthermore based on the use of the CAM-B3LYP hybrid exchange-correlation functional [42] in combination with the aug-cc-pVDZ basis set.

The calculated solvent shifts are shown in Figure 3.3 together with the experimental solvent shift [43]. The first columns, that is, M0, M1, M2 M3 show the trends of the shifts with increasing order of the multipole expansion. These force fields do not model solvent polarization and are only used to investigate the effects of the higher order multipoles on the

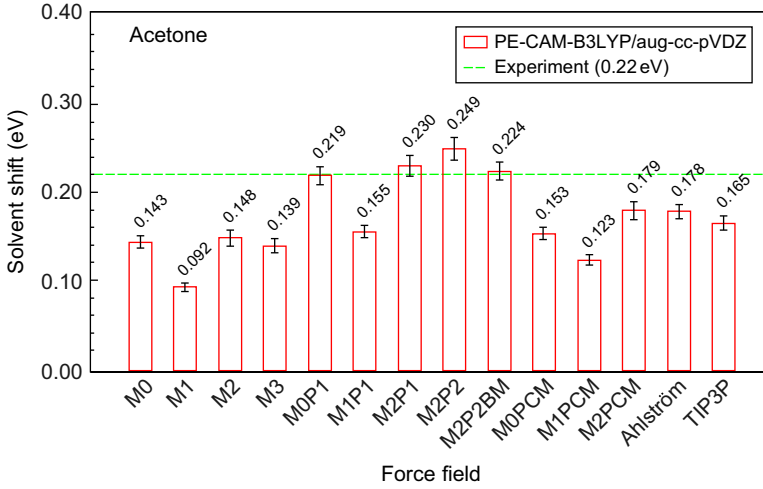

Figure 3.3 The gas-to-aqueous solvent shift of the lowest $n \rightarrow \pi^*$ excitation energy in acetone. Results from Ref. [6].

excitation energies. In all cases, we observe a large effect from both the dipole and quadrupole moments. On the other hand, the inclusion of octopoles leads to very small changes, indicating that we are converged at the quadrupole level with respect to the order of the permanent multipole moments. Thereby, we find a clear correlation between the trends here and the behavior of the force fields in terms of how well they reproduce the QM electrostatic potential. Note that the shifts at the M0 and M2 and M3 levels in general are very similar due to the fact that the effects from the dipole and quadrupole moments tend to cancel each other. Introducing distributed isotropic polarizabilities in addition to the permanent multipoles, that is, M0P1, M1P1 and M2P1, leads to an increase of the solvent shifts. Comparing the shifts calculated at the M2P1 level to the M2 level shows that the solvent shifts are increased from about 50% in the case of $n \rightarrow \pi^*$ transitions in acetone. This clearly shows that induction effects have a significant impact on the solvent shifts and therefore must be taken into account. The use of distributed anisotropic polarizabilities, that is, the M2P2 force field, only gives small improvements as compared to the distributed isotropic polarizabilities. This can probably be explained by the rather small degree of anisotropy of the water molecule. Using the most sophisticated LoProp force field, M2P2BM, decreases the solvent shifts by a small amount as compared to the M2P2 force field. This indicates that the M2P2 force field has a tendency to overestimate the induction effects, at least in the present case. It is interesting to note that the M0P1 force field performs rather well compared with the full M2P2BM force field. Therefore, we find that an acceptable approximation would be to use the M0P1 force field that captures the main parts of the electrostatics and induction effects due to a water solvent on the vertical excitation energies.

Recognizing that it is necessary to include the induction effects, a natural question is whether an explicit inclusion of polarization is needed or if it is sufficient to have implicit polarization by using enhanced permanent multipoles as obtained in the MXPCM force fields. Using the M0PCM, M1PCM, and M2PCM force fields, we obtained larger solvent shifts as compared to the M0, M1, and M2 force fields. Still, these MXPCM-based solvent shifts are not as accurate as in the case where explicit polarization has been taken into account, which clearly illustrates the importance of explicit polarization effects.

3.3. Nuclear magnetic resonance chemical shifts

As a further example on the use of the PE scheme, we discuss the calculation of NMR shielding constants for molecules in solution. More specifically, we will focus on the case of pyridine in water solution [44]. The NMR calculations presented here are based on the use of the PBE0 functional combined with the 6-311++G(2d,2p) basis set. The PE-DFT results for the NMR

Table 3.1 The statistically averaged ^{15}N NMR isotropic shielding constants of pyridine in aqueous solution, σ^N, (in ppm) and corresponding solvent shifts, $\Delta\sigma^N$. Experimental data is taken from Ref. [46]. Results from Ref. [44]

QM part	σ^N	$\Delta\sigma^N$
NC_5H_5	-62.0 ± 0.3	28.9 ± 0.3
$NC_5H_5 + 1\ H_2O$	-64.7 ± 0.6	26.2 ± 0.6
$NC_5H_5 + 2\ H_2O$	-65.9 ± 0.6	25.0 ± 0.6
exp.		29.7

shielding constants of pyridine are the statistical averages over 200 molecular configurations extracted from a molecular dynamics simulation [44]. The NMR results will be restricted to the use of the Ahlström water potential. Below, we will address the issue of hydrogen bonding between pyridine and water and investigate the effect of this on the NMR shielding constant of the nitrogen nucleus in pyridine. Our interest is in the gas-to-aqueous solution shifts of the ^{15}N NMR isotropic shielding constants denoted by $\Delta\sigma^N$.

The computed gas-to-aqueous solution shifts of the ^{15}N NMR isotropic shielding constant of pyridine are collected in Table 3.1. We begin by considering the pyridine molecule at the selected PBE0/6-311++G(2d,2p) level and all water molecules treated classically using the Ahlström force field. The obtained solvent shift in σ^N of 28.9 $\pm$ 0.3 ppm is in fairly good agreement with the experimental result of 29.7 ppm. As discussed in the previous sections, the Ahlström water potential is not completely converged with respect to the electrostatic potential. Furthermore, it is well known that nonelectrostatic solute–solvent effects may have a nonnegligible effect on NMR shielding tensors. Therefore, we include in the QM region one or two explicit water molecules selected from the molecular dynamics simulation. For these extended PE-DFT calculations, we observe a decrease in the predicted result from the solvent shift of the ^{15}N NMR isotropic shielding constant of 2.7 ppm when one water molecule is included in the QM region and a further 1.2 ppm when two water molecules are treated by quantum mechanics. Overall, it is seen that inclusion of explicit water molecules at the QM level leads to slightly underestimated results for the predicted solvent shifts. The reason for this decreased agreement between experiment and theory is most likely to be found in the neglect of rovibrational averaging on $\Delta\sigma^N$, something which has previously been proved to be important in some cases [45].

3.4. Second hyperpolarizabilities

As a final example of the applicability of the PE-DFT method, we consider in this section calculations related to a higher order response property, namely,

the second hyperpolarizability. The calculation of accurate nonlinear optical (NLO) properties of molecules in the condensed phase is a challenging task for theorists. The importance of models capable of predicting molecular NLO properties may be attributed to the potential design of new materials geared toward application in optical devices. Microscopically, the relevant optical properties are, to lowest orders, the first and second frequency-dependent hyperpolarizabilities. Accurate calculations of these hyperpolarizabilities have, for atoms and small molecules in the gas phase, become feasible using either finite field (FF) techniques or the theory of response functions. The latter approach, which will be used here, offers some advantages: (1) it is numerically stable, (2) it requires fewer calculations to be performed by the user and, (3) it is general in the sense that all frequency combinations of the properties may be addressed, that is, third harmonic generation (THG) second hyperpolarizabilities may be calculated, which is not possible using an approach based on the FF scheme.

Table 3.2 contains results of the rotationally averaged static second hyperpolarizability, $\gamma_{||}$, of a methanol molecule in liquid methanol. The calculations are based on the use of the CAM-B3LYP hybrid exchange-correlation functional in combination with the very flexible d-aug-cc-pVTZ basis set and the M2P2BM water potential. Generally, calculations of hyperpolarizabilities require the use of basis sets with very diffuse basis functions that reflect the choice of this specific basis set. The results are furthermore based on averaging of 100 snapshots extracted from a 4-ns long molecular dynamics simulation. From the results in Table 3.2, we observe a significant dependence on the force field used in the PE calculations. Clearly, the results based on the M0 potential lead to underestimated results for the second hyperpolarizability. In accordance with the results previously discussed for the electronic excitation energies, we observe a convergence in the solvent electrostatic potential at the level of quadrupoles, that is, inclusion of octopoles lead to changes that are almost within the statistical uncertainty

Table 3.2 Statistically averaged static mean second hyperpolarizabilities of methanol in methanol solution. Results are in a.u.

Force field	$\gamma_{\|\|}$
M0	3724 ± 46
M1	4541 ± 55
M2	4374 ± 74
M3	4494 ± 72
M2P1	5028 ± 109
M2P2	4902 ± 112
M2P2BM	4967 ± 97

Table 3.3 Statistically averaged static and dynamic third harmonic generation mean second hyperpolarizabilities of methanol in vacuum or in methanol solution. Results are in a.u. and are based on the use of the M2P2BM water potential

$\gamma_{\|\|}(-3\omega;\omega,\omega,\omega)$	$\omega = 0.0000$	$\omega = 0.0239$	$\omega = 0.0656$
Vacuum	3853	4151	7573
Methanol solution	4970 ± 54	5400 ± 62	11001 ± 223

of the averaged property. Explicit inclusion of polarization effects is seen to enhance this fourth-order property markedly. On the other hand, the different descriptions of the polarizability, that is, isotropic or anisotropic, lead to deviations that again are within the statistical error.

The dispersion related to the second hyperpolarizability of methanol is shown in Table 3.3 where we have included, in addition to the rotationally averaged static second hyperpolarizability, results related to the THG at two different frequencies. As opposed to the results in Table 3.2, we have, for the results presented in Table 3.3, used 400 snapshots. This has been done in order to reduce the statistical error. From this table, we observe that in the low frequency limit, the dispersion is similar in both gas phase and in solution, whereas an enhanced dispersion is observed in the higher frequency region for methanol in solution as compared to methanol in the gas phase. This increase in dispersion also results in an increase in the statistical error related to the second hyperpolarizability, that is, because of local anisotropies in the environment, each methanol molecule possesses a slightly different dispersion in the second hyperpolarizability, leading to an increase in the statistical error. As seen from the results in Table 3.3, the solvent shift, that is, the difference between the second hyperpolarizability in solution and in gas phase, is always positive; again, we observe that the solvent shift is similar for the lower frequencies, whereas it increases for frequencies lying in the higher frequency regime. Thus, a frequency-dependent solvent shift may only be estimated from its static limit, but for high-level results, the frequency dependence of the solvent shift needs to be included explicitly.

4. CONCLUSION

We have presented a general review of polarizable embedding within quantum chemistry. Special attention has been given to the theoretical background of polarizable embedding and its extension to the calculation of general molecular properties within the framework of time-dependent density functional theory. In addition, we have presented a few selected applications limited to the use of polarizable embedding for the description of solute molecular properties. Current investigations based on the use

of polarizable embedding are in the direction of applications for biological relevant molecules such as photoactive proteins and rational approaches to the design of general materials.

ACKNOWLEDGMENT

The authors thank the Danish Center for Scientific Computing for computational resources. J.K. thanks the Danish Natural Science Research Council/The Danish Councils for Independent Research and the Lundbeck Foundation for financial support.

REFERENCES

[1] A. Warshel, M. Levitt, Theoretical studies of enzymic reactions: Dielectric, electrostatic and steric stabilization of the carbonium ion in the reaction of lysozyme, J. Mol. Biol. 103 (1976) 227.
[2] U.C. Singh, P.A. Kollman, A combined ab initio quantum mechanical and molecular mechanical method for carrying out simulations on complex molecular systems: Applications to the ch3cl + cl- exchange reaction and gas phase protonation of polyethers, J. Comput. Chem. 7 (1986) 718.
[3] M.J. Field, P.A. Bash, M. Karplus, A combined quantum mechanical and molecular mechanical potential for molecular dynamics simulations, J. Comput. Chem. 11 (1990) 700.
[4] J. Gao, X. Xia, A priori evaluation of aqueous polarization effects through monte carlo qm-mm simulations, Science 258 (1992) 631.
[5] H. Lin, D.G. Truhlar, Qm/mm: What have we learned, where are we, and where do we go from here? Theor. Chem. Acc. 117 (2007) 185.
[6] J.M. Olsen, K. Aidas, J. Kongsted, Excited states in Solution through Polarizable Embedding, J. Chem. Theory Comput. 6 (2010) 3721.
[7] T. Rocha-Rinza, K. Sneskov, O. Christiansen, U. Ryde, J. Kongsted, Unraveling the similarity of the photoabsorption of deprotonated p-coumaric acid in the gas phase and within the photoactive yellow protein, Phys. Chem. Chem. Phys. 13 (2011) 1585.
[8] J. Applequist, J.R. Carl, K.-K. Fung, Atom dipole interaction model for molecular polarizability, application to polyatomic molecules and determination of atom polarizabilities, J. Am. Chem. Soc. 94 (1972) 2952.
[9] P.N. Day, J.H. Jensen, M.S. Gordon, S.P. Webb, W.J. Stevens, M. Krauss, D. Garmer, H. Basch, D. Cohen, An effective fragment method for modeling solvent effects in quantum mechanical calculations, J. Chem. Phys. 105 (1996) 1968.
[10] M.S. Gordon, M.A. Freitag, P. Bandyopadhyay, J.H. Jensen, V. Kairys, W.J. Stevens, The effective fragment potential method: A QM-based MM approach to modeling environmental effects in chemistry, J. Phys. Chem. A 105 (2001) 293.
[11] M.S. Gordon, L.V. Slipchenko, H. Li, J.H. Jensen, The effective fragment potential: A general method for predicting intermolecular interactions, Ann. Rep. Comput. Chem. 3 (2007) 177.
[12] W.L. Jorgensen, Special issue on polarization, J. Chem. Theory Comput. 3 (2007) 1877.
[13] H. Yu, W.F. van Gunsteren, Accounting for polarization in molecular simulation, Comput. Phys. Commun. 172 (2005) 69.
[14] DALTON, A molecular electronic structure program, Release 2.0, 2005. See http://www.kjemi.uio.no/software/dalton/dalton.html

[15] T. Helgaker, P. Jørgensen, J. Olsen, Molecular Electronic-Structure Theory, Wiley, Chichester, England, 2000.
[16] A.J. Stone, The Theory of Intermolecular Forces, Oxford University Press Inc, New York, 1996.
[17] P. Sałek, O. Vahtras, T. Helgaker, H. Ågren, Density-functional theory of linear and nonlinear time-dependent molecular properties, J. Chem. Phys. 117 (2002) 9630.
[18] B. Jansik, P. Salek, D. Jonsson, O. Vahtras, H. Ågren, Cubic response functions in time-dependent density functional theory, J. Chem. Phys. 122 (2005) 054107.
[19] J. Tomasi, B. Mennucci, R. Cammi, Quantum mechanical continuum solvation models, Chem. Rev. 105 (2005) 2999.
[20] R. Cammi, L. Frediani, B. Mennucci, K. Ruud, Multiconfigurational self-consistent field linear response for the polarizable continuum model: Theory and application to ground and excited-state polarizabilities of para-nitroaniline in solution, J. Chem. Phys. 119 (2003) 5818.
[21] K.V. Mikkelsen, P. Jorgensen, H.J.Aa. Jensen, A multiconfigurational self-consistent reaction field response method, J. Chem. Phys. 100 (1994) 6597.
[22] K.O. Sylvester-Hvid, K.V. Mikkelsen, D. Jonsson, P. Norman, H. Ågren, Nonlinear optical response of molecules in a nonequilibrium solvation model, J. Chem. Phys. 109 (1998) 5576.
[23] J. Olsen, P. Jørgensen, Linear and nonlinear response functions for an exact state and for an mcscf state, J. Chem. Phys. 82 (1985) 3235.
[24] C.B. Nielsen, O. Christiansen, K.V. Mikkelsen, J. Kongsted, Density functional self-consistent quantum mechanics/molecular mechanics theory for linear and nonlinear molecular properties: Applications to solvated water and formaldehyde, J. Chem. Phys. 126 (2007) 154112.
[25] S. Yoo, F. Zahariev, S. Sok, M.S. Gordon, Solvent effects on optical properties of molecules: A combined time-dependent density functional theory/effective fragment potential approach, J. Chem. Phys. 129 (2008) 144112.
[26] J. Gauss, Effects of electron correlation in the calculation of nuclear magnetic resonance chemical shifts, J. Chem. Phys. 99 (1993) 3629.
[27] T. Helgaker, M. Jaszunski, K. Ruud, Ab initio methods for the calculation of nmr shielding and indirect spin-spin coupling constants, Chem. Rev. 99 (1999) 293.
[28] K. Ruud, T. Helgaker, R. Kobayashi, P. Jørgensen, K. Bak, H. Jensen, Multiconfigurational self-consistent field calculations of nuclear shieldings using london atomic orbitals, J. Chem. Phys. 100 (1994) 8178.
[29] F. London, Théorie quantique des courants interatomiques dans les combinaisons aromatiques, J. Phys. Radium 8 (1937) 397.
[30] H. Hameka, Theory of magnetic properties of molecules with particular emphasis on the hydrogen molecule, Rev. Mod. Phys. 34 (1962) 87.
[31] R. Ditchfield, A gauge-invariant lcao method for n.m.r. chemical shifts, Mol. Phys. 27 (1974) 789.
[32] K. Wolinski, J. Hinton, P. Pulay, Efficient implementation of the gauge-independent atomic orbital method for nmr chemical shift calculations, J. Am. Chem. Soc. 112 (1990) 8251.
[33] Q. Cui, M. Karplus, Molecular properties from combined qm/mm methods. 2. Chemical shifts in large molecules, J. Phys. Chem. B 104 (2000) 3721.
[34] J.R. Cheeseman, G.W. Trucks, T.A. Keith, M.J. Frisch, A comparison of models for calculating nuclear magnetic resonance shielding tensors, J. Chem. Phys. 104 (1996) 5497.
[35] J. Kongsted, C.B. Nielsen, K.V. Mikkelsen, O. Christiansen, K. Ruud, Nuclear magnetic shielding constants of liquid water: Insights from hybrid quantum mechanics/molecular mechanics models, J. Chem. Phys. 126 (2007) 034510.
[36] T. Helgaker, P. Jørgensen, An electronic hamiltonian for origin independent calculations of magnetic properties, J. Chem. Phys. 95 (1991) 2595.
[37] L. Gagliardi, R. Lindh, G. Karlström, Local properties of quantum chemical systems: The loprop approach, J. Chem. Phys. 121 (2004) 4494.

[38] G. Karlström, R. Lindh, P.-Å. Malmqvist, B.O. Roos, U. Ryde, V. Veryazov, P.-O. Widmark, M. Cossi, B. Schimmelpfennig, P. Neograd y, L. Seijo, Molcas: A program package for computational chemistry, Comp. Mat. Sci. 28 (2003) 222.
[39] P. Ahlström, A. Wallqvist, S. Engström, B. Jönsson, A molecular dynamics study of polarizable water, Mol. Phys. 68 (1989) 563.
[40] W.L. Jorgensen, Quantum and statistical mechanical studies of liquids. 10. Transferable intermolecular potential functions for water, alcohols, and ethers, application to liquid water, J. Am. Chem. Soc. 103 (1981) 335.
[41] P. Söderhjelm, J.W. Krogh, G. Karlström, U. Ryde, R. Lindh, Accuracy of distributed multipoles and polarizabilities: Comparison between the loprop and mpprop models, J. Comput. Chem. 28 (2007) 1083.
[42] T. Yanai, D.P. Tew, N.C. Handy, A new hybrid exchangecorrelation functional using the coulomb-attenuating method (cam-b3lyp), Chem. Phys. Lett. 393 (2004) 51.
[43] I. Renge, Solvent dependence of n-pi* absorption in acetone, J. Phys. Chem. A 113 (2009) 10678.
[44] K. Aidas, K.V. Mikkelsen, J. Kongsted, Modelling spectroscopic properties of large molecular systems, the combined density functional theory/molecular mechanics approach, J. Chem. Meth. Sci. Eng. 7 (2007) 135.
[45] J. Kongsted, K. Ruud, Solvent effects on zero-point vibrational corrections to optical rotations and nuclear magnetic resonance shielding constants, Chem. Phys. Lett. 451 (2008) 226.
[46] M. Witanowski, L. Stefaniak, G.A. Webb, Annual Reports on NMR Spectroscopy, Vol. 25, Academic Press: London, 1993.